

A New Constraint on the Optical Depth from the Reionization History Independent of CMB Large-Scale E-Mode Polarization

YUTA KAGEURA ^{1,2} MASAMI OUCHI ^{3,1,4,5} FUMIHIRO NAOKAWA ^{2,6} HIROYA UMEDA ^{1,2} AKINORI MATSUMOTO,^{1,2}
YUICHI HARIKANE ¹ MINAMI NAKANE ^{1,2} AND TRAN THI THAI ³

¹*Institute for Cosmic Ray Research, The University of Tokyo, 5-1-5 Kashiwanoha, Kashiwa, Chiba 277-8582, Japan*

²*Department of Physics, Graduate School of Science, The University of Tokyo, 7-3-1 Hongo, Bunkyo, Tokyo 113-0033, Japan*

³*National Astronomical Observatory of Japan, 2-21-1 Osawa, Mitaka, Tokyo 181-8588, Japan*

⁴*Astronomical Science Program, Graduate Institute for Advanced Studies, SOKENDAI, 2-21-1 Osawa, Mitaka, Tokyo 181-8588, Japan*

⁵*Kavli Institute for the Physics and Mathematics of the Universe (Kavli IPMU, WPI), The University of Tokyo, 5-1-5 Kashiwanoha, Kashiwa, Chiba, 277-8583, Japan*

⁶*Research Center for the Early Universe, The University of Tokyo, Bunkyo-ku, Tokyo 113-0033, Japan*

ABSTRACT

Recent studies report a mild discrepancy between baryon acoustic oscillation (BAO) and cosmic microwave background (CMB) measurements within the Λ CDM framework. This discrepancy could be explained if the optical depth τ inferred from the CMB large-scale E-mode polarization is underestimated, which may be biased by foreground-subtraction or instrumental systematics. In this work, we present a determination of τ independent of the large-scale E-mode polarization, using the latest measurements of the redshift evolution of the neutral hydrogen fraction $x_{\text{H}_1}(z)$, which is constrained by Lyman- α forest and damping-wing absorption measurements at $z \sim 5\text{--}14$, based on ground-based optical and JWST observations. Combining $x_{\text{H}_1}(z)$ with the Planck CMB power spectra excluding the large-scale E-mode polarization, we obtain $\tau = 0.0552^{+0.0019}_{-0.0026}$, a stringent constraint consistent with the previous CMB results including the large-scale E-mode. We also evaluate a potential systematic error in our method associated with absorption modeling, obtaining $\tau = 0.0552^{+0.0075}_{-0.0049}$. Using this constraint on τ , we resolve the degeneracy in the $\tau\text{--}\Omega_{\text{m}}$ plane and find a 2.4σ tension with the DESI DR2 BAO results, thereby confirming the claimed mild discrepancy suggestive of physics beyond Λ CDM. Finally, we derive an upper limit on the sum of neutrino masses, $\Sigma m_{\nu} < 0.0550$ (0.0717) eV at the 95% (99%) confidence level. This limit favors the normal mass ordering and, when combined with the lower limits from neutrino oscillation experiments, yields a further constraint, $\Sigma m_{\nu} = 0.0594^{+0.0113}_{-0.0007}$ eV. However, the cosmological upper limit and the oscillation-based lower limit show a mild 2.2σ tension, providing an independent indication of possible physics beyond Λ CDM.

Keywords: Cosmic microwave background radiation (322) — Cosmological parameters (339) — Neutrino masses (1102) — Reionization (1383)

1. INTRODUCTION

The Cosmic Microwave Background (CMB) is one of the most powerful probes for determining cosmological parameters. In the base- Λ CDM model, the temperature and polarization power spectra, as well as CMB lensing measurements, are described by five cosmolog-

ical parameters and the CMB optical depth to reionization, τ (Planck Collaboration et al. 2020a). The parameter τ quantifies the Thomson scattering of CMB photons by free electrons after cosmic reionization, with earlier (later) reionization history corresponding to a larger (smaller) value of τ . A precise determination of τ is crucial because τ and other cosmological parameters both affect the amplitude of the power spectra, leading to parameter degeneracies.

Large-scale CMB E-mode polarization anisotropies are highly sensitive to τ (Planck Collaboration et al.

Corresponding author: Yuta Kageura
kageura@icrr.u-tokyo.ac.jp

2016a). However, measuring this signal is challenging because the expected CMB polarization signal is more than two orders of magnitude weaker than the TT (temperature) power spectrum. Both instrumental systematic effects and foreground residuals must be suppressed to very low levels to accurately extract the true CMB signal (Planck Collaboration et al. 2020b). These observational challenges are evident in the history of τ estimates.

The Wilkinson Microwave Anisotropy Probe (WMAP) mission was the first to constrain τ based on the TE (temperature-polarization cross) power spectrum, obtaining a large value of $\tau = 0.166_{-0.071}^{+0.076}$ in its 1-yr results (Spergel et al. 2003). Subsequent analyses reduced this value to $\tau = 0.089 \pm 0.014$ in the final 9-yr results, incorporating the TE and EE (polarization) power spectra (Bennett et al. 2013).

The Planck mission further revised τ downward to $\tau = 0.079 \pm 0.017$ in its 2015 results, which included large-scale TE and EE measurements, or to $\tau = 0.063 \pm 0.014$ after incorporating CMB lensing (Planck Collaboration et al. 2016b). In the Planck 2018 results, τ was determined to be $\tau = 0.0544 \pm 0.0073$ using the small-scale TT, TE, EE power spectra, large-scale TT and EE power spectra, and CMB lensing measurements (Planck Collaboration et al. 2020a).

The large-scale polarization measurements from Planck may be affected by instrumental systematics (Planck Collaboration et al. 2016c), and efforts to mitigate these systematics are ongoing. In the Planck 2018 analysis, the `SimAll` likelihood was used for the low-multipole (i.e., large-scale, $l < 30$) polarization power spectrum (Planck Collaboration et al. 2020a). To address known instrumental effects, the `SRoll2` likelihood (Delouis et al. 2019) was developed. Based on Planck PR4 data, an alternative likelihood, `LoLLiPoP`, was constructed (Tristram et al. 2021, 2022). These likelihoods yield slightly different τ estimates (Pagano et al. 2020; Tristram et al. 2024). Thus, measuring the low-multipole polarization from Planck is still challenging. We also note that current ground-based CMB results, including those from ACT (Louis et al. 2025) and SPT (Camphuis et al. 2025), can be affected by such systematic effects in Planck, since they rely on Planck results for the large-scale.

Moreover, several recent studies have proposed that τ may take higher values than those inferred from Planck (Allali et al. 2025; Jhaveri et al. 2025; Liu et al. 2025; Sailer et al. 2025). Since τ and Ω_m are negatively correlated, a higher value, $\tau \sim 0.09$, can alleviate the mild tension in Ω_m between the baryon acoustic oscillation (BAO) measurements from the Dark Energy Spectro-

scopic Instrument (DESI) DR2 and Planck within the Λ CDM model (Jhaveri et al. 2025; Sailer et al. 2025). In addition, several studies extending beyond the standard scenario have shown that the low-multipole Planck results can be consistent with $\tau \sim 0.09$ (Naokawa et al. 2024; Namikawa 2025; Tan & Komatsu 2025).

Taking these observational challenges into account, we are strongly motivated to measure τ independently of the CMB large-scale E-mode polarization. In this paper, we focus on the redshift evolution of the neutral hydrogen fraction, $x_{\text{H}_1}(z)$, derived from quasar (QSO) and galaxy observations at $z \gtrsim 5$, as an alternative probe to constrain τ (Elbers 2025; Garcia-Gallego et al. 2025; Paoletti et al. 2025; Sims et al. 2025). A higher x_{H_1} leads to stronger Ly α absorption in these spectra, allowing $x_{\text{H}_1}(z)$ to be constrained from the observations.

At $z \sim 5 - 6$, Gunn-Peterson absorption (Gunn & Peterson 1965) in the Lyman-series (e.g., Ly α) forest of QSO spectra provides constraints on x_{H_1} . For example, dark gaps and the fraction of dark pixels with no detectable transmission in the Lyman-series forests are used to constrain $x_{\text{H}_1}(z)$ (McGreer et al. 2015; Zhu et al. 2022; Jin et al. 2023; Davies et al. 2026). Although Gunn-Peterson absorption cannot probe $z \gtrsim 6$ owing to saturation, much weaker Lyman- α damping-wing absorption due to natural broadening (i.e., the uncertainty principle in energy and time) can constrain higher neutral fractions, $x_{\text{H}_1} \sim 0.1 - 1$. At $z \sim 6 - 7$, Lyman- α damping-wing absorption in QSO and gamma-ray burst (GRB) spectra is used to measure $x_{\text{H}_1}(z)$ (Totani et al. 2006, 2014; Wang et al. 2020; Greig et al. 2022, 2024; Durovčíková et al. 2024; Fausey et al. 2025). The damping-wing absorption of Ly α emission from galaxies is also used to investigate $x_{\text{H}_1}(z)$ through the evolution of the Ly α luminosity function (LF) (Wold et al. 2022; Umeda et al. 2025b), Ly α emitter (LAE) clustering (Sobacchi & Mesinger 2015; Ouchi et al. 2018; Umeda et al. 2025b), and the Ly α equivalent width (EW) distribution (Mason et al. 2018, 2019a; Jung et al. 2020; Whitler et al. 2020; Bolan et al. 2022). The James Webb Space Telescope (JWST) has further enabled us to constrain reionization history at $z \gtrsim 8$, through the detection of damping-wing absorption in Lyman-break galaxy (LBG) spectra and the redshift evolution of the Ly α EW distribution (Nakane et al. 2024; Tang et al. 2024; Jones et al. 2025; Kageura et al. 2025; Mason et al. 2025; Napolitano et al. 2025; Umeda et al. 2025a).

We need to combine $x_{\text{H}_1}(z)$ with other cosmological probes to derive τ and some other cosmological parameters. In practice, Paoletti et al. (2025) and Sims et al. (2025) constrained τ using the reionization history, obtaining $\tau = 0.052 \pm 0.002$ and $\tau = 0.0542_{-0.0028}^{+0.0017}$, respec-

tively. However, because they combined CMB measurements that include the large-scale E-mode polarization, these results are not independent of potential issues in the low-multipole CMB polarization.

Elbers (2025) obtained $\tau = 0.0492^{+0.0014}_{-0.0030}$ independently of the CMB by combining BAO measurements, Big Bang nucleosynthesis (BBN), and reionization history. This result is consistent with the Planck results and smaller than $\tau \sim 0.09$, which has been proposed as a possible resolution of the CMB-BAO tension. However, because BAO measurements are not dependent on τ , combining reionization history with BAO does not improve the constraint on Ω_m . Therefore, the combination of reionization history and CMB provides a more powerful probe to test whether the CMB-BAO tension in Ω_m exists, by solving the degeneracy between τ and Ω_m . Measurements that exclude BAO are also important to avoid the impact of potential systematic errors in BAO measurements.

In this study, therefore, we present constraints on τ by combining reionization history with CMB measurements that exclude the large-scale E-mode polarization data. Through this combination, we test whether the CMB-BAO tension persists without large-scale E-mode measurements, which may be biased by instrumental or foreground-subtraction systematics. We incorporate the latest constraints on reionization history derived from the redshift evolution of Ly α emission observed with JWST and Subaru, in contrast to previous studies, while carefully excluding duplicate measurements.

This combination can simultaneously tighten constraints on other cosmological parameters that are degenerate with τ in the CMB alone. In addition, we perform further analyses combining CMB, BAO, and reionization history data to study models beyond Λ CDM. We consider dynamical dark energy, which has been proposed as a possible resolution of the CMB-BAO tension, and the sum of neutrino masses, Σm_ν , which is degenerate with τ . We also investigate potential systematic errors in measurements of the reionization history, which can bias cosmological parameters inferred from this combination.

This paper is organized as follows. Section 2 describes the data used to constrain cosmological parameters. Section 3 presents the reconstruction of the reionization history based on Lyman- α forest data and QSO/galaxy Lyman- α damping-wing absorption measurements. In Section 4, we describe constraints on the base- Λ CDM model. Section 5 explores constraints on the dynamical dark energy model. Finally, we present constraints on the sum of neutrino masses in Section 6. Section 7 summarizes our findings.

2. DATA

In this work, we primarily use constraints on cosmic reionization history derived from galaxy and quasar observations at $z \gtrsim 5$ (Section 2.1) and CMB measurements (Section 2.2). Data from other cosmological observations and high-energy experiments (Sections 2.3 and 2.4) are also used to compare with our results for the base- Λ CDM model and to jointly constrain extensions to the base- Λ CDM model.

2.1. Constraints on Cosmic Reionization History

We use constraints on x_{H_1} at various redshifts derived from galaxy and quasar observations at $z \gtrsim 5$ reported in the literature. In addition to Ly α forest and GRB/QSO/LBG damping-wing absorption measurements, we incorporate the latest constraints on reionization history derived from the redshift evolution of Ly α emission observed with JWST and Subaru, which were not used in previous studies (Elbers 2025; Paoletti et al. 2025; Sims et al. 2025). We note that many x_{H_1} measurements are based on the same observational data. For example, the LBG spectrum used in Curtis-Lake et al. (2023) is included in the sample of Umeda et al. (2025a). Although these duplicated measurements were used in some previous studies, we avoid duplication and use the following latest results from the literature:

- Ly α damping-wing absorption of GRBs at $z = 5.9 - 6.3$ (Totani et al. 2006, 2014; Fausey et al. 2025)
- Ly α damping-wing absorption of QSOs at $z = 6.0 - 7.5$ (Greig et al. 2022; Ďurovčíková et al. 2024)
- Ly α damping-wing absorption of LBGs at $z = 5 - 13$ (Umeda et al. 2025a)
- Clustering properties of Ly α emitters at $z = 5 - 7$ (Umeda et al. 2025b)
- Evolution of the Ly α luminosity function at $z = 5 - 7$ (Wold et al. 2022; Umeda et al. 2025b)
- Evolution of the Ly α EW distribution at $z = 5 - 14$ (Mason et al. 2019b; Jung et al. 2020; Whitler et al. 2020; Bolan et al. 2022; Kageura et al. 2025)
- Dark gaps in the Ly β forest at $z = 5.5 - 6.0$ (Zhu et al. 2022)
- Fraction of dark pixels in the Lyman-series forests at $z = 4.9 - 6.2$ (Davies et al. 2026)

Although the reionization history is well constrained at $z = 5 - 8$, constraints are weaker at higher redshifts, especially at $z > 10$. To ensure that the reionization history remains a monotonically increasing function, we assume $x_{\text{H}_1} > 0.999$ (1σ lower limit) at $z = 15.0$, following Elbers (2025). We note that the neutral fraction at $z = 15$ is close to unity in most reionization models (Ishigaki et al. 2018; Finkelstein et al. 2019; Mason et al. 2019a; Naidu et al. 2020; Muñoz et al. 2024; Asthana et al. 2025; Kageura et al. 2025; Qin et al. 2025).

2.2. Cosmic Microwave Background

We use publicly available CMB datasets (Table 1). Large-scale E-mode polarization data are excluded from our analysis because instrumental systematic effects and foreground residuals could significantly impact these measurements (Planck Collaboration et al. 2020b; Sailer et al. 2025). For the small-scale ($l \geq 30$) temperature (TT), polarization (EE), and cross (TE) power spectra, we use the `CamSpec` likelihood based on the Planck PR4 (NPIPE) maps (Efstathiou & Gratton 2021; Rosenberg et al. 2022). For the large-scale ($l < 30$) temperature power spectrum, we use the `Commander` likelihood from the Planck PR3 release (Planck Collaboration et al. 2020c)⁷. For CMB lensing, we use the v1.2 lensing likelihood from the ACT Collaboration, which combines the ACT DR6 and Planck PR4 results (Caron et al. 2022; Madhavacheril et al. 2024; Qu et al. 2024)⁸. Hereafter, we denote this dataset as CMB (w/o lowE). In contrast, we denote the dataset including the large-scale E-mode power spectrum as CMB (w/ lowE).

2.3. BAO

We use the DESI DR2 BAO likelihood (Abdul Karim et al. 2025a,b)⁹. The combination of all subsets of the DESI BAO data is included in our analysis.

2.4. Neutrino Oscillations

Results from neutrino oscillation experiments are used to jointly constrain the sum of neutrino masses Σm_ν . Esteban et al. (2024) derived the neutrino mass-squared differences, Δm_{21}^2 and Δm_{31}^2 , using various experimental data, including SK1-4, T2K, and NoVA, through NuFIT 6.0¹⁰. We use the two-dimensional $\Delta\chi^2$ values for Δm_{21}^2

⁷ The PR3 and PR4 likelihoods are publicly available as internal likelihoods in `Cobaya` (<https://github.com/CobayaSampler/cobaya>)

⁸ https://github.com/ACTCollaboration/act_dr6_lenslike

⁹ <https://data.desi.lbl.gov/public/papers/y3/bao-cosmo-params/README.html>

¹⁰ <http://www.nu-fit.org>

and Δm_{31}^2 to jointly constrain Σm_ν in combination with reionization history, CMB, and BAO data.

3. RECONSTRUCTING REIONIZATION HISTORY

To derive the CMB optical depth τ , the reionization history $x_{\text{H}_1}(z)$ as a function of redshift is required. To reconstruct the reionization history, we adopt Gaussian process regression. Gaussian process regression is a non-parametric method for reconstructing a function from a finite set of data points without assuming any specific physical model, and it can be regarded as a generalization of binning (Lodha et al. 2025). Using constraints on the neutral fraction x_{H_1} at various redshifts $\mathbf{z} = (z_1, z_2, \dots, z_n)$ (Section 2.1), x_{H_1} values at new redshift points $\mathbf{z}^* = (z_1^*, z_2^*, \dots, z_{n'}^*)$ can be obtained as a posterior distribution in a Bayesian framework. Unlike approaches that construct a reionization model by solving an ionization differential equation from high to low redshift (or vice versa), our method infers the values of x_{H_1} at all redshift points simultaneously. The Gaussian process prior further correlates nearby redshift points, favoring similar x_{H_1} values at similar redshifts and thereby yielding a smooth, continuous reionization history consistent with the data. We calculate the posterior distribution $p(x_{\text{H}_1}(\mathbf{z}^*)|\{x_{\text{H}_1}\})$ using Gaussian process regression, where $\{x_{\text{H}_1}\}$ denotes the full set of constraints on $x_{\text{H}_1}(\mathbf{z})$. We use the Markov Chain Monte Carlo (MCMC) method with the `emcee` package (Foreman-Mackey et al. 2013) to perform the regression, with 62 chains and 10^5 steps. See Appendix A for details of the regression methodology. For Gaussian process reconstruction of the reionization history, see also Elbers (2025). The reconstructed reionization history is shown in Figure 1. In the reconstructed history, reionization primarily occurs at $z \sim 6 - 8$, which is consistent with previous astrophysical results (Naidu et al. 2020; Mathee et al. 2022; Kageura et al. 2025; Shimizu et al. 2025). In comparison, under an instantaneous reionization scenario, an optical depth of $\tau \sim 0.09$ implies that reionization occurs at $z \sim 11$. However, our results indicate that the neutral hydrogen fraction remains as high as $x_{\text{H}_1}(z) \sim 0.9$ at $z \sim 11$.

4. CONSTRAINTS ON THE BASE- Λ CDM MODEL

4.1. Likelihood and Methodology

We first constrain cosmological parameters within Λ CDM cosmology. In our analysis, we simultaneously fit five cosmological parameters and the reionization history using the CMB likelihoods and the Gaussian process regression results. For the cosmological parameters, we include the baryon density $\omega_b = \Omega_b h^2$, cold dark matter density $\omega_c = \Omega_c h^2$, Hubble constant H_0 , primordial

Table 1. CMB likelihoods used in this work.

Likelihood	Power spectrum	Name in Cobaya	Reference
CamSpec	Planck small-scale ($l \geq 30$) TT+TE+EE	planck_NPIPE_highl_CamSpec.TTTEEE	(1, 2)
Commander	Planck large-scale ($l < 30$) TT	planck_2018_lowl.TT_clik	(3)
Lensing	ACT+Planck CMB lensing	act_dr6_lenslike.ACTDR6LensLike	(4, 5, 6)

NOTE—References. (1)Efstathiou & Gratton (2021), (2)Rosenberg et al. (2022), (3)Planck Collaboration et al. (2020c), (4)Carron et al. (2022), (5)Madhavacheril et al. (2024), (6)Qu et al. (2024)

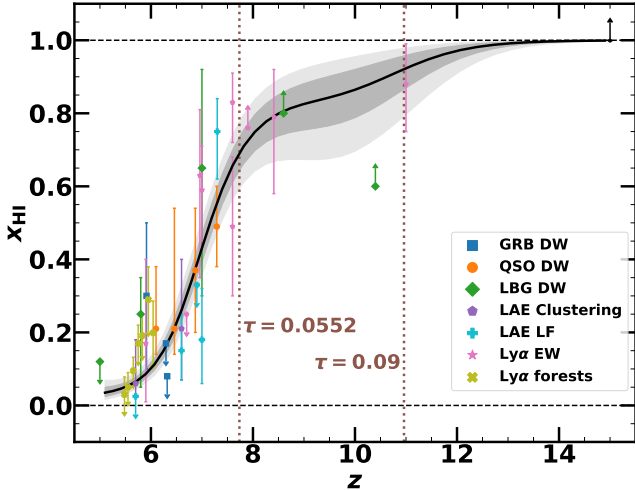


Figure 1. Cosmic reionization history reconstructed via Gaussian process regression. The black line represents the median reionization history, while the gray shaded regions show the 68% (dark gray) and 95% (light gray) posterior ranges. We also present x_{HI} estimates based on various methods used in this work: Ly α damping-wing absorption of GRBs (blue squares; Totani et al. 2006, 2014; Fausey et al. 2025), QSOs (orange circles; Greig et al. 2022; Dřurovčíková et al. 2024), LBGs (green diamonds; Umeda et al. 2025a), LAE clustering (purple pentagons; Umeda et al. 2025b), Ly α luminosity function (cyan pluses; Wold et al. 2022; Umeda et al. 2025b), Ly α EW distribution (pink stars; Mason et al. 2019b; Jung et al. 2020; Whitler et al. 2020; Bolan et al. 2022; Kageura et al. 2025), and Ly α / β forests (olive crosses; Zhu et al. 2022; Davies et al. 2026). The brown dotted lines indicate the redshift corresponding to instantaneous reionization with $\tau = 0.09$ and $\tau = 0.0552$, for $\Omega_b h^2 = 0.02237$, $\Omega_c h^2 = 0.1200$, and $h = 0.6736$. We note that the instantaneous reionization redshift $z = 7.73$ for $\tau = 0.0552$ differs from the midpoint of reionization $z_{\text{mid}} = 7.19$, since the actual reionization history is not instantaneous.

curvature power spectrum amplitude $\ln(10^{10} A_s)$, and spectral index n_s to fit the CMB power spectra. The sum of neutrino masses is fixed at $\Sigma m_\nu = 0.06$ eV. For the reionization history, we use x_{HI} values at ten redshift points, $x_{\text{HI}}(z_1), \dots, x_{\text{HI}}(z_{10})$ as fitting parameters. We set these redshift points at equal intervals in $\log(1+z)$ -space, spanning $z_1 = 5$ to $z_{10} = 15$. We confirm that a 10-point sampling is sufficient for the integra-

tion in Equation (2) to converge and that τ is calculated with an accuracy of 10^{-4} , which is significantly smaller than the statistical error. The posterior distribution of the cosmological parameters $\boldsymbol{\theta}$ and reionization history $x_{\text{HI}}(\mathbf{z}^*)$, given the CMB data d_{CMB} and reionization constraints $\{x_{\text{HI}}\}$, is expressed as

$$\begin{aligned} \log p(\boldsymbol{\theta}, x_{\text{HI}}(\mathbf{z}^*) | d_{\text{CMB}}, \{x_{\text{HI}}\}) \\ = \log p(x_{\text{HI}}(\mathbf{z}^*) | \{x_{\text{HI}}\}) + \log p(d_{\text{CMB}} | \boldsymbol{\theta}, x_{\text{HI}}(\mathbf{z}^*)) \\ + \log p(\boldsymbol{\theta}) + \text{const.} \end{aligned} \quad (1)$$

The first term represents the posterior distribution from the Gaussian process. The second term is the CMB likelihood. In this framework, we directly fit the reionization history and do not treat τ as an explicit fitting parameter. Instead, τ is derived from ω_b , ω_c , H_0 , and the reionization history using the following formula:

$$\tau = \frac{3c\omega_b X_p \sigma_T \times 100 \text{ km/s}}{8\pi G m_p} \times \int dz \frac{(1 - x_{\text{HI}}(z))(1 + z)^2}{\sqrt{(\omega_b + \omega_c)((1 + z)^3 - 1) + h^2}} \left(1 + \frac{\eta Y_p}{4X_p}\right), \quad (2)$$

where c is the speed of light, X_p is the hydrogen fraction, Y_p is the helium fraction, σ_T is the Thomson-scattering cross section, G is the gravitational constant, and m_p is the proton mass. The parameter η accounts for additional electrons supplied by helium reionization. Following Planck Collaboration et al. (2020a), we assume that the first helium reionization occurs contemporaneously with hydrogen reionization, and the second helium reionization takes place at $z = 3.5$ (i.e., $\eta = 1$ at $z > 3.5$ and $\eta = 2$ at $z \leq 3.5$).

The CMB likelihood (Table 1) is evaluated using the five cosmological parameters and the derived τ . Theoretical CMB angular power spectra are calculated using CAMB (Lewis et al. 2000; Howlett et al. 2012). We use cobaya (Torrado & Lewis 2019, 2021) to evaluate the CMB likelihood. The third term is the prior distribution of the cosmological parameters. We adopt flat priors on the cosmological parameters used in Planck Collaboration et al. (2014) and Planck Collaboration

Table 2. Parameter means and 68% credible intervals for the base- Λ CDM model from CMB and reionization history.

Parameter	CMB (w/o lowE)	CMB (w/ lowE)	CMB (w/o lowE)+ $x_{\text{H}_1}(z)$
τ	0.072 ± 0.016	0.0539 ± 0.0073	$0.0552^{+0.0019}_{-0.0026}$
$\ln(10^{10} A_s)$	3.074 ± 0.028	3.043 ± 0.013	$3.0451^{+0.0055}_{-0.0062}$
n_s	0.9666 ± 0.0047	0.9634 ± 0.0040	0.9638 ± 0.0038
$\Omega_b h^2$	0.02226 ± 0.00015	0.02218 ± 0.00013	0.02218 ± 0.00013
$\Omega_c h^2$	0.1190 ± 0.0013	0.1200 ± 0.0011	0.11993 ± 0.00099
H_0 [km s $^{-1}$ Mpc $^{-1}$]	67.61 ± 0.60	67.14 ± 0.47	67.17 ± 0.44
Ω_m	0.3104 ± 0.0082	0.3169 ± 0.0065	0.3165 ± 0.0061
σ_8	0.8205 ± 0.0092	0.8106 ± 0.0051	0.8115 ± 0.0036
S_8	0.834 ± 0.010	0.833 ± 0.011	0.833 ± 0.011
H_{0rd} [km s $^{-1}$]	9891 ± 81	9973 ± 100	9896 ± 76

et al. (2020a). Although our primary results are based on CMB (w/o lowE) and reionization history $x_{\text{H}_1}(z)$, we also derive results using CMB (w/o lowE) alone for comparison. The posterior distributions are sampled using the MCMC method with `emcee` with 10^4 steps and $2 \times$ (number of parameters) walkers.

4.2. Cosmological Parameters

In Figure 2 and Table 2 we show the posterior distributions of the cosmological parameters and τ . The MCMC samples are analyzed and plotted using `GetDist` (Lewis 2025). For comparison, we also show the results from CMB (w/ lowE) based on the publicly available MCMC chains provided by the DESI Collaboration¹¹. By combining reionization history data with CMB (w/o lowE), we obtain a stringent constraint on the optical depth,

$$\tau = 0.0552^{+0.0019}_{-0.0026} \quad (\text{CMB (w/o lowE)} + x_{\text{H}_1}(z)). \quad (3)$$

This result is consistent with the constraint from CMB large-scale E-mode polarization,

$$\tau = 0.0539 \pm 0.0072 \quad (\text{CMB (w/ lowE)}). \quad (4)$$

Without reionization history, we obtain

$$\tau = 0.072 \pm 0.016 \quad (\text{CMB (w/o lowE)}). \quad (5)$$

Incorporating $x_{\text{H}_1}(z)$ data improves the estimate of τ by a factor of 7. We compare our constraint on τ with literature values in Figure 3.

Because τ is degenerate with other cosmological parameters, constraints on other cosmological parameters also improve when $x_{\text{H}_1}(z)$ data are included. In particular, the constraint on the primordial power spectrum amplitude A_s significantly improves when $x_{\text{H}_1}(z)$

is included, since the amplitude of the small-scale CMB power spectrum scales with $A_s e^{-2\tau}$. We obtain

$$\ln(10^{10} A_s) = 3.0451^{+0.0055}_{-0.0062} \quad (\text{CMB (w/o lowE)} + x_{\text{H}_1}(z)), \quad (6)$$

which is consistent with the lowE result, $\ln(10^{10} A_s) = 3.043 \pm 0.013$ (CMB (w/ lowE)). By solving the degeneracy between A_s and τ , our constraint on A_s is improved by a factor of 5 relative to that from CMB (w/o lowE) alone, $\ln(10^{10} A_s) = 3.074 \pm 0.028$.

Because increases in τ and n_s both suppress power at high- l , these two parameters are also correlated (McDonough & Ferreira 2025). We obtain constraints on n_s as

$$n_s = 0.9638 \pm 0.0038 \quad (\text{CMB (w/o lowE)} + x_{\text{H}_1}(z)), \quad (7)$$

which is consistent with the lowE result, $n_s = 0.9634 \pm 0.0040$ (CMB (w/ lowE)). The value of n_s from CMB (w/o lowE)+ $x_{\text{H}_1}(z)$ is in agreement with the Higgs, Starobinsky, and exponential α -attractor inflation models (Kallosh & Linde 2025).

4.3. Comparison with BAO Measurements

As shown in Figure 2, H_0 , $\Omega_c h^2$, and τ are correlated with each other. Consequently, the precise constraint on τ leads to improved constraints on the Hubble constant H_0 , matter density Ω_m , and sound horizon scale r_d as follows:

$$H_0 = 67.17 \pm 0.44 \text{ [km s}^{-1} \text{ Mpc}^{-1}\text{]} \quad (\text{CMB (w/o lowE)} + x_{\text{H}_1}(z)) \quad (8)$$

$$\Omega_m = 0.3165 \pm 0.0061 \quad (\text{CMB (w/o lowE)} + x_{\text{H}_1}(z)) \quad (9)$$

¹¹ <https://data.desi.lbl.gov/public/papers/y3/bao-cosmo-params/README.html>

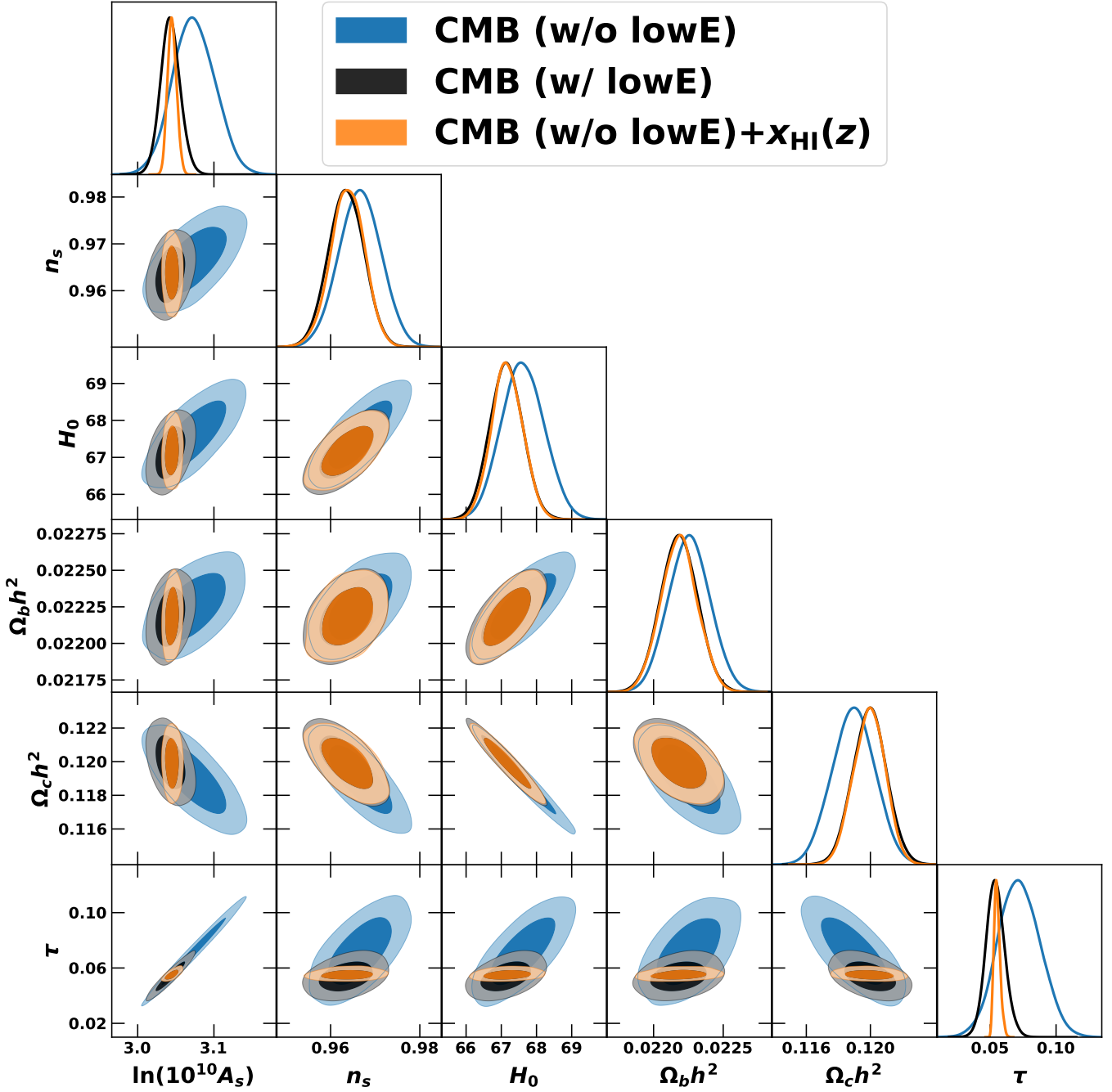


Figure 2. Constraints on cosmological parameters and τ for the Λ CDM model. The orange contours represent constraints derived from CMB Planck TTTEEE and Planck+ACT lensing and cosmic reionization history, excluding low- l EE. The blue and black contours indicate constraints obtained from CMB (w/o lowE) and CMB (w/ lowE), respectively. The dark and light contours show the 68% and 95% regions, respectively.

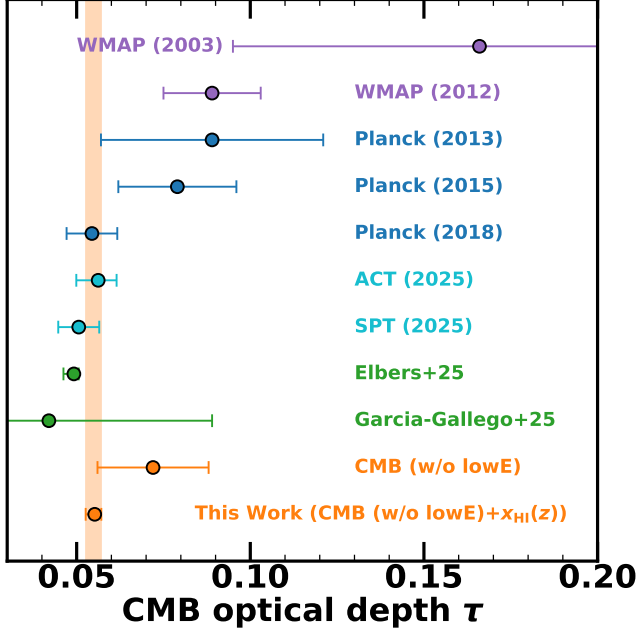


Figure 3. Comparison of our τ values with those from previous studies. The orange circles show our τ values from CMB (w/o lowE) and CMB (w/o lowE)+ $x_{\text{HI}}(z)$. The purple and blue points indicate τ values from WMAP (Spergel et al. 2003; Bennett et al. 2013) and Planck (Planck Collaboration et al. 2014, 2016b, 2020a), respectively. The cyan circles show results from ACT (Louis et al. 2025) and SPT (Campsma et al. 2025) combined with Planck data. The green circles represent τ constraints from Elbers (2025) based on reionization history, BAO, and BBN, and from Garcia-Gallego et al. (2025) based on the Ly α forest.

$$H_0 r_d = 9896 \pm 76 \text{ [km s}^{-1}\text{]} \quad (\text{CMB (w/o lowE)} + x_{\text{HI}}(z)). \quad (10)$$

We show these constraints in Figure 4. We compare our results with those from BAO measurements. DESI DR2 finds $\Omega_m = 0.2975 \pm 0.0086$, and $H_0 = 68.51 \pm 0.58 \text{ [km s}^{-1} \text{ Mpc}^{-1}\text{]}$ with a BBN prior on ω_b (Abdul Karim et al. 2025a). These Ω_m and H_0 values are fully consistent with those obtained from CMB (w/o lowE) alone. In contrast, the results from CMB (w/o lowE)+ $x_{\text{HI}}(z)$ exhibit mild discrepancies with the BAO constraints, with a 1.8σ difference for both Ω_m and H_0 . To further examine whether the results based on CMB (w/o lowE)+ $x_{\text{HI}}(z)$ are in tension with DESI DR2 BAO measurements, we evaluate the discrepancy in the $H_0 r_d - \Omega_m$ plane (Figure 5). We use the MCMC chains of the posterior distributions and covariance matrices of cosmological parameters that are publicly provided by

the DESI Collaboration¹². Following Abdul Karim et al. (2025a), we compute the relative χ^2 between CMB (w/o lowE)+ $x_{\text{HI}}(z)$ and BAO as

$$\chi^2 = (\mathbf{p}_C - \mathbf{p}_B)^T (\text{Cov}_C + \text{Cov}_B)^{-1} (\mathbf{p}_C - \mathbf{p}_B), \quad (11)$$

where \mathbf{p}_C (\mathbf{p}_B) and Cov_C (Cov_B) represent the $(H_0 r_d, \Omega_m)$ values and covariance matrices from CMB (w/o lowE)+ $x_{\text{HI}}(z)$ (BAO), respectively. We convert this χ^2 value to a probability-to-exceed (PTE) value and find a 2.4σ tension between CMB (w/o lowE)+ $x_{\text{HI}}(z)$ and BAO measurements. This result is consistent with the 2.3σ discrepancy between BAO and CMB including large-scale E-mode polarization reported by the DESI Collaboration (Abdul Karim et al. 2025a). Although the BAO measurements are consistent with CMB excluding large-scale polarization measurements that may be affected by instrumental and foreground systematics, the inclusion of the reionization history helps to solve the degeneracies between τ and Ω_m , as well as between τ and $H_0 r_d$. This confirms the CMB-BAO tension without relying on large-scale E-mode polarization measurements. Since the impact of the Ω_m - τ degeneracy is largely removed, future BAO measurements will be required to investigate this tension with higher statistical precision.

4.4. The Fluctuation Amplitude

As discussed in Section 4.2, the CMB optical depth τ and primordial power spectrum amplitude A_s are strongly correlated. A precise determination of τ using reionization history thus leads to a simultaneous improvement in the constraint on A_s . Under the Λ CDM model, A_s can be converted into the fluctuation amplitude at $z = 0$, σ_8 . We compute σ_8 using the CAMB code and obtain

$$\sigma_8 = 0.8115 \pm 0.0036 \quad (\text{CMB (w/o lowE)} + x_{\text{HI}}(z)). \quad (12)$$

Our result is consistent with the CMB constraint including large-scale E-mode polarization, $\sigma_8 = 0.8106 \pm 0.0051$ (CMB (w/o lowE)). Our constraint is ~ 3 times tighter than that obtained using CMB (w/o lowE) alone, $\sigma_8 = 0.8205 \pm 0.0092$ (CMB (w/o lowE)).

Galaxy clustering measurements provide an independent constraint on the fluctuation amplitude. We compare our results with data from the Dark Energy Survey (DES) Y3. For this comparison, we use the cosmology chains for the fiducial Λ CDM $3 \times 2\text{pt}$

¹² <https://data.desi.lbl.gov/public/papers/y3/bao-cosmo-params/README.html>

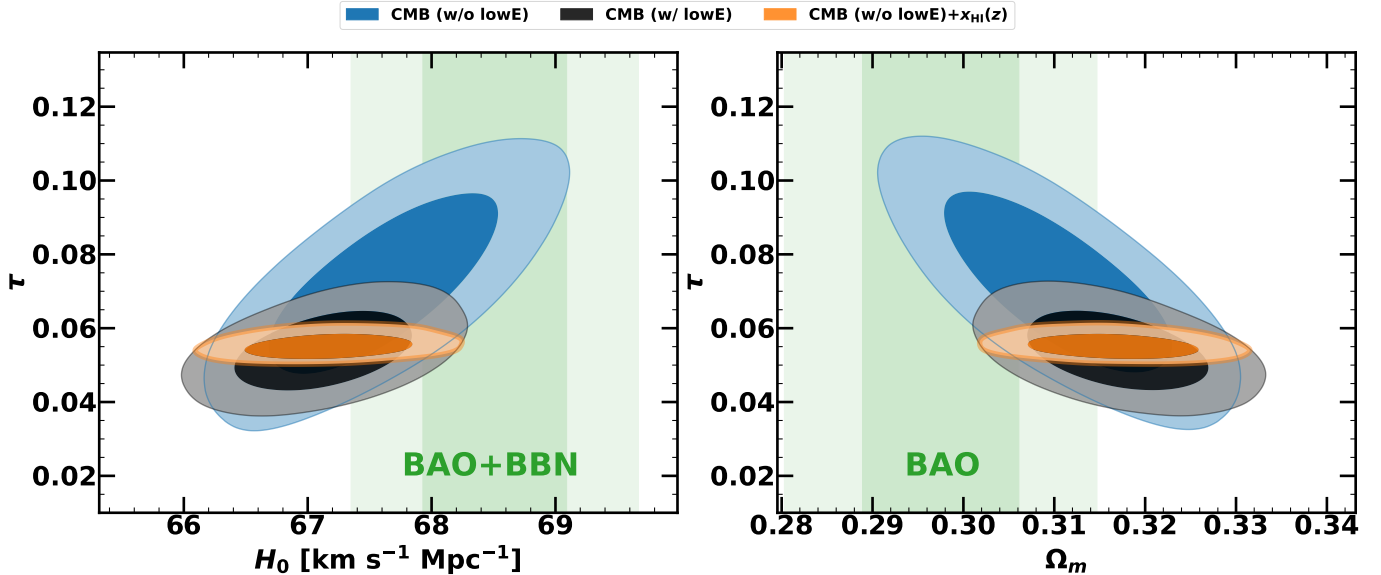


Figure 4. Constraints on H_0 and Ω_m for the Λ CDM model. The blue, black, and orange contours show results based on CMB (w/o lowE), CMB (w/ lowE), and CMB (w/o lowE)+ $x_{\text{HI}}(z)$, respectively. The green region for Ω_m indicates constraints from DESI DR2 BAO measurements, while the green region for H_0 shows results from DESI DR2 BAO data with a BBN prior on ω_b . Contours show the 68% and 95% regions.

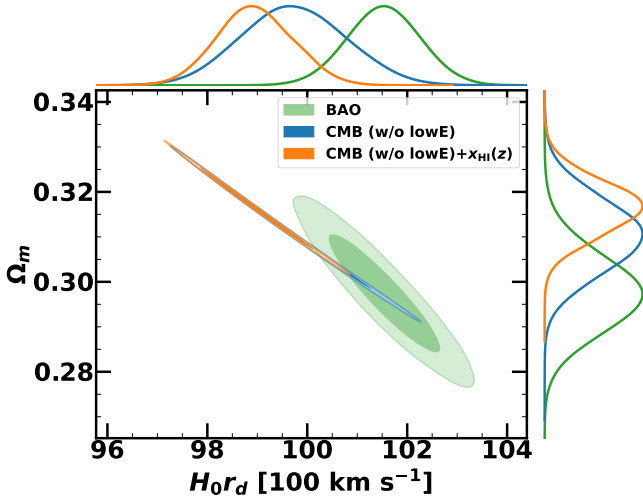


Figure 5. Constraints on H_{0rd} and Ω_m for the Λ CDM model from DESI DR2 BAO (green), CMB (w/o lowE) (blue), and CMB (w/o lowE)+ $x_{\text{HI}}(z)$ (orange). The result including reionization history in this work is consistent with the CMB (w/ lowE) constraint and is in 2.4σ tension with the DESI DR2 BAO measurements. Contours show the 68% and 95% regions.

likelihood, which combines two-point correlation functions of cosmic shear, galaxy clustering, and the cross-correlation of source galaxy shear with lens galaxy positions, galaxy-galaxy lensing (The Dark Energy Survey Collaboration 2005; Flaugher et al. 2015; Dark Energy

Survey Collaboration et al. 2016; Abbott et al. 2022a,b; Amon et al. 2022; Secco et al. 2022)¹³.

In Figure 6, we present our results together with the DES Y3 constraints. We calculate $S_8 = \sigma_8 \sqrt{\Omega_m}/0.3$ and find

$$S_8 = 0.833 \pm 0.011 \quad (\text{CMB (w/o lowE)} + x_{\text{HI}}(z)). \quad (13)$$

Our S_8 value is consistent with the lowE result of $S_8 = 0.833 \pm 0.011$ (CMB (w/ lowE)) and is larger than the DES Y3 measurement, $S_8 = 0.776 \pm 0.018$, by 2.7σ . In contrast, our result is consistent with the $3 \times 2\text{pt}$ analysis of Year 3 Hyper Suprime-Cam (HSC-Y3) and the cosmic shear constraints from the Kilo-Degree Survey (KiDS), which report $S_8 = 0.775^{+0.043}_{-0.038}$ (Miyatake et al. 2023; More et al. 2023; Sugiyama et al. 2023)¹⁴ and $S_8 = 0.815^{+0.016}_{-0.021}$ (Wright et al. 2024, 2025)¹⁵, respectively. Further investigations are needed to clarify the presence of the S_8 tension.

4.5. Possible Systematics in the Determination of τ

Our reconstruction of the reionization history relies on measurements of x_{HI} inferred from Ly α damping-wing absorption in the spectra of galaxies and QSOs. A

¹³ <https://des.ncsa.illinois.edu/releases/y3a2/Y3key-products>

¹⁴ Cosmological chains are publicly available at <https://hsc-release.mtk.nao.ac.jp/doc/index.php/s19a-shape-catalog-pdr3/>.

¹⁵ Cosmological chains are publicly available at <https://kids.strw.leidenuniv.nl/>.

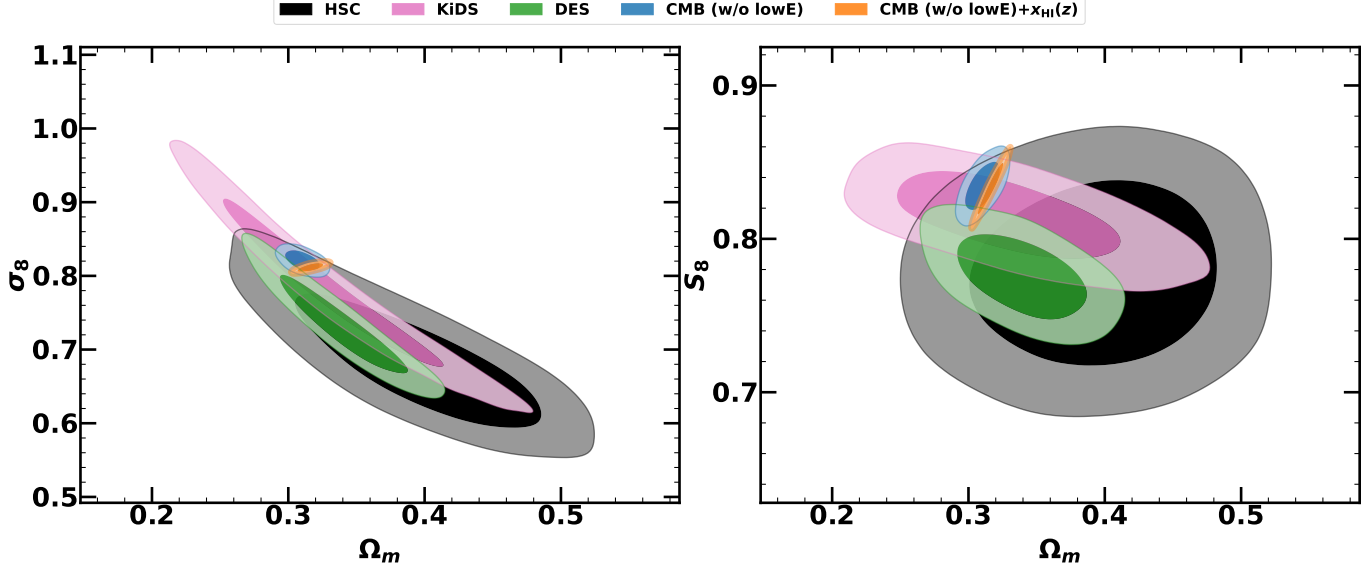


Figure 6. Constraints on σ_8 and S_8 for the Λ CDM model from HSC-Y3 (black), KiDS-Legacy (pink), DES Y3 (green), CMB (w/o lowE) (blue), and CMB (w/o lowE)+ $x_{\text{HI}}(z)$ (orange). The S_8 value obtained from CMB (w/o lowE)+ $x_{\text{HI}}(z)$ is 2.7σ higher than the DES Y3 constraint, while remaining consistent with the HSC-Y3, KiDS-Legacy, and CMB (w/o lowE) results. Contours show the 68% and 95% regions.

key caveat is that such inferences are intrinsically model dependent. The damping-wing strength is sensitive not only to the mean neutral fraction but also to the characteristic size distribution of ionized bubbles. Therefore, assumptions about the IGM topology can bias the inferred x_{HI} . Kageura et al. (2025) quantified this effect by estimating x_{HI} using a standard model and an extreme scenario with very large ionized bubbles. They found that the inferred x_{HI} can shift by up to $\sim 7\%$ between these models. For individual data points, this uncertainty is smaller than the statistical errors. However, a coherent bias of comparable magnitude affecting all measurements could propagate non-negligibly into the determination of τ .

To account for this potential systematics, we propagate a $\sim 7\%$ modeling uncertainty in the x_{HI} values and obtain $\tau = 0.0552^{+0.0075}_{-0.0049}$ (systematics). Under this conservative treatment, the systematic uncertainty exceeds the statistical uncertainty while remaining comparable to the uncertainty in the large-scale CMB polarization constraints ($\tau = 0.0539 \pm 0.0072$; CMB (w/o lowE)). Therefore, our discussion of the CMB-BAO tension is not qualitatively affected by this possible modeling systematics.

We note that there are potential systematic biases that are not included in the discussion above. For example, the intrinsic spectra prior to IGM absorption must be assumed to evaluate the Ly α damping-wing absorption. In many studies, galaxy/QSO spectra at $z \lesssim 5$ are used to model the intrinsic spectra at the Epoch of

Reionization (EoR). However, the intrinsic properties of galaxies and QSOs at the EoR may differ from those at lower redshifts. For example, Rinaldi et al. (2023) found the typical H α EW of galaxies evolve as $\propto (1+z)^{2.1}$, potentially suggesting that Ly α and UV continuum emission also evolve with redshift.

The resolution of simulations can also affect the inferred value of x_{HI} . To account for the inhomogeneous ionization state of the IGM during the EoR, many studies estimate x_{HI} by comparing observed galaxy and QSO properties with IGM simulations. However, capturing the inhomogeneity of reionization requires simulation volumes on Gpc scales, larger than typical ionized bubbles, while small-scale physics is also known to play a major role in regulating the progress of reionization and the absorption of background radiation. For example, Cain et al. (2024) showed that calculations of Ly α forest power spectrum have not yet converged even in simulations with a high spatial resolution of ~ 2 kpc per cell, and it remains unclear which observables are affected by simulation resolution and to what extent.

Quantitative assessments of these potential sources of systematic uncertainty therefore require further investigation in future work.

5. DYNAMICAL DARK ENERGY

In Section 4.3, we show that our CMB (w/o lowE)+ $x_{\text{HI}}(z)$ results for the $(H_0 r_d - \Omega_m)$ parameters are in 2.4σ tension with DESI DR2 BAO. This tension is consistent with the 2.3σ CMB-BAO tension including E-mode polarization (Abdul Karim et al. 2025a) and

Table 3. Parameter means and 68% credible intervals for the $w_0 w_a$ model from CMB, BAO, and reionization history.

Parameter	CMB (w/o lowE)	CMB (w/o lowE)+BAO	CMB (w/ lowE)+BAO	CMB (w/o lowE)+BAO+ $x_{\text{H}_1}(z)$
w_0	$-1.12^{+0.43}_{-0.48}$	$-0.51^{+0.21}_{-0.24}$	-0.42 ± 0.21	$-0.55^{+0.17}_{-0.26}$
w_a	$-0.5^{+1.4}_{-1.2}$	$-1.44^{+0.73}_{-0.58}$	-1.75 ± 0.58	$-1.40^{+0.70}_{-0.47}$
τ	0.065 ± 0.018	$0.065^{+0.015}_{-0.017}$	0.0527 ± 0.0071	$0.0556^{+0.0018}_{-0.0027}$
$\ln(10^{10} A_s)$	3.060 ± 0.033	$3.060^{+0.026}_{-0.029}$	3.038 ± 0.013	3.0437 ± 0.0060
n_s	0.9658 ± 0.0047	$0.9662^{+0.0037}_{-0.0042}$	0.9644 ± 0.0037	0.9649 ± 0.0034
$\Omega_b h^2$	0.02226 ± 0.00015	0.02226 ± 0.00014	0.02221 ± 0.00012	0.02222 ± 0.00013
$\Omega_c h^2$	0.1191 ± 0.0014	0.1190 ± 0.0011	0.11960 ± 0.00083	0.11940 ± 0.00077
H_0 [km s $^{-1}$ Mpc $^{-1}$]	$75.2^{+7.2}_{-13}$	64.3 ± 1.9	$63.6^{+1.7}_{-2.1}$	$64.8^{+2.4}_{-1.6}$
Ω_m	$0.264^{+0.065}_{-0.078}$	$0.344^{+0.020}_{-0.023}$	0.353 ± 0.021	$0.339^{+0.016}_{-0.027}$
σ_8	$0.881^{+0.063}_{-0.101}$	0.791 ± 0.018	$0.781^{+0.015}_{-0.018}$	$0.792^{+0.020}_{-0.014}$
S_8	$0.810^{+0.045}_{-0.029}$	0.846 ± 0.013	$0.846^{+0.013}_{-0.012}$	0.841 ± 0.012
H_{0rd} [km s $^{-1}$]	11090^{+1000}_{-1900}	9484 ± 290	9378^{+250}_{-310}	9558^{+360}_{-240}

may suggest cosmology beyond Λ CDM, although further investigations are needed to confirm the tension. One possible scenario to resolve this tension is the $w_0 w_a$ (dynamical dark energy) model (Abdul Karim et al. 2025a). In this section, we constrain cosmological parameters for the dynamical dark energy model with the equation-of-state parameter,

$$w = w_0 + (1 - a)w_a, \quad (14)$$

where a is the scale factor, and w_0 and w_a are constant parameters. In Λ CDM cosmology, $w_0 = -1$ and $w_a = 0$. Here, we vary these two parameters and adopt flat priors for w_0 and w_a with ranges of $-3 < w_0 < 1$ and $-3 < w_a < 2$, following Abdul Karim et al. (2025a). We use three datasets to constrain the dynamical dark energy model: (i) CMB (w/o lowE), (ii) CMB (w/o lowE) and DESI DR2 BAO, and (iii) CMB (w/o lowE), DESI DR2 BAO, and reionization history $x_{\text{H}_1}(z)$. We follow the method in Section 4.1 and obtain constraints on cosmological parameters (Table 3). For comparison, we also show results from CMB (w/ lowE)+BAO based on the publicly available MCMC chains provided by the DESI Collaboration.

The derived equation-of-state parameters are

$$w_0 = -0.55^{+0.17}_{-0.26} \quad w_a = -1.40^{+0.70}_{-0.47} \quad (\text{CMB (w/o lowE) + BAO + } x_{\text{H}_1}(z)). \quad (15)$$

In Figure 7, we show the marginalized posterior distributions of the (w_0, w_a) parameters. From CMB (w/o lowE) measurements, the (w_0, w_a) values are consistent with the Λ CDM model. However, when BAO and reionization history $x_{\text{H}_1}(z)$ are included, the posterior distribution deviates from the Λ CDM values of $(w_0, w_a) = (-1, 0)$. Following Abdul Karim et al. (2025a), we compute the χ^2 value between the best-fit (w_0, w_a)

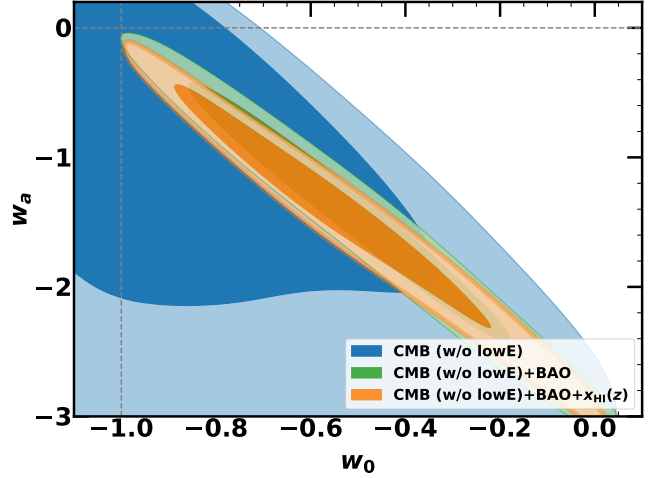


Figure 7. Marginalized posterior distributions of the (w_0, w_a) parameters from CMB (w/o lowE) (blue), +BAO (green), and $+x_{\text{H}_1}(z)$ (orange). The dashed lines indicate $w_0 = -1$ and $w_a = 0$. The Λ CDM model is disfavored at 2.1σ significance by CMB (w/o lowE)+BAO+ $x_{\text{H}_1}(z)$, consistent with the CMB (w/ lowE)+BAO result reported by Abdul Karim et al. (2025a). Contours show the 68% and 95% regions.

and $(-1, 0)$. With this procedure, the Λ CDM model is disfavored at 2.1σ significance by the CMB (w/o lowE)+BAO+ $x_{\text{H}_1}(z)$ data. This result is consistent with the lowE result, $w_0 = -0.42 \pm 0.21$ and $w_a = -1.75 \pm 0.58$ (CMB (w/ lowE)+BAO), and aligns with previous studies (Abdul Karim et al. 2025a; Elbers 2025). Although this result requires further validation, if confirmed, it may indicate that dark energy is not a cosmological constant but instead reflects physics beyond a simple cosmological constant, such as an axion-like field (Tada & Terada 2024).

Table 4. Parameter means and 68% credible intervals for the base- Λ CDM model+ Σm_ν from CMB, BAO, and reionization history. We quote 95% upper limits for Σm_ν .

Parameter	CMB (w/o lowE)	CMB (w/o lowE)+BAO	CMB (w/ lowE)+BAO	CMB (w/o lowE)+BAO+ $x_{\text{H}_1}(z)$
Σm_ν [eV]	< 0.445	< 0.121	< 0.0649	< 0.0550
τ	$0.084^{+0.018}_{-0.022}$	0.083 ± 0.015	$0.0582^{+0.0065}_{-0.0075}$	$0.0572^{+0.0021}_{-0.0042}$
$\ln(10^{10} A_s)$	$3.098^{+0.034}_{-0.041}$	3.092 ± 0.026	$3.049^{+0.012}_{-0.014}$	$3.0465^{+0.0060}_{-0.0084}$
n_s	0.9666 ± 0.0046	$0.9705^{+0.0033}_{-0.0039}$	0.9683 ± 0.0034	0.9680 ± 0.0036
$\Omega_b h^2$	0.02225 ± 0.00015	0.02237 ± 0.00013	0.02232 ± 0.00012	0.02233 ± 0.00012
$\Omega_c h^2$	0.1190 ± 0.0013	$0.11744^{+0.00085}_{-0.00071}$	0.11804 ± 0.00064	0.11807 ± 0.00063
H_0 [km s $^{-1}$ Mpc $^{-1}$]	$66.5^{+1.7}_{-1.0}$	68.49 ± 0.32	68.37 ± 0.29	68.40 ± 0.29
Ω_m	$0.325^{+0.012}_{-0.023}$	0.2991 ± 0.0040	0.3009 ± 0.0037	$0.3006^{+0.0034}_{-0.0037}$
σ_8	$0.803^{+0.027}_{-0.015}$	0.8284 ± 0.0092	$0.8168^{+0.0065}_{-0.0057}$	$0.8163^{+0.0052}_{-0.0039}$
S_8	0.835 ± 0.011	0.8272 ± 0.0092	0.8180 ± 0.0077	0.8171 ± 0.0070
$H_0 r_d$ [km s $^{-1}$]	9804^{+260}_{-160}	10120 ± 52	10100 ± 49	10100 ± 48

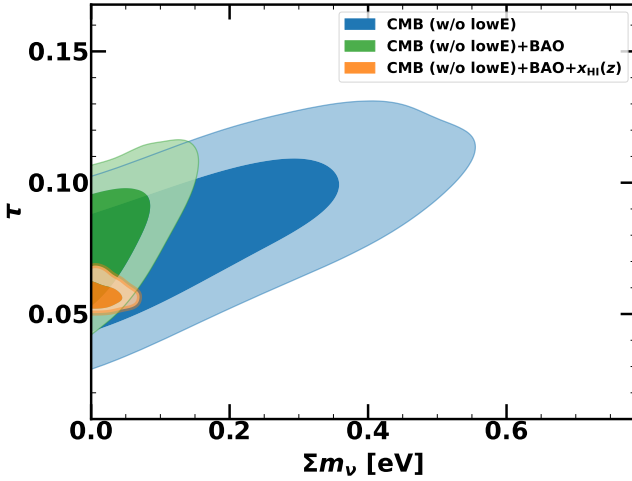


Figure 8. Marginalized posterior distributions of the $(\Sigma m_\nu - \tau)$ parameters from CMB (w/o lowE) (blue), +BAO (green), and $+x_{\text{H}_1}(z)$ (orange). A 95% (99%) upper limit of $\Sigma m_\nu < 0.0550$ (0.0717) eV is obtained from CMB (w/o lowE)+BAO+ $x_{\text{H}_1}(z)$. A similar upper limit of $\Sigma m_\nu < 0.0649$ (0.0906) eV (95% (99%)) is obtained from CMB (w/ lowE)+BAO. Contours show the 68% and 95% regions.

6. SUM OF NEUTRINO MASSES

The sum of neutrino masses Σm_ν is positively correlated with τ (Elbers et al. 2025; Jhaveri et al. 2025). As shown in Section 4.2, raising τ increases the inferred A_s and hence the amount of CMB lensing. On the other hand, a larger Σm_ν suppresses the growth of structure through free-streaming, thereby decreasing the CMB lensing signal (Du et al. 2025). Therefore, it is important to investigate how the cosmic reionization history affects Σm_ν . In Section 4, we fix the sum of neutrino masses to $\Sigma m_\nu = 0.06$ eV. In this section, we allow Σm_ν to vary and derive an upper limit on Σm_ν within Λ CDM cosmology. We assume a flat prior on Σm_ν over the range

of [0, 5] eV. As in Section 5, we use three datasets to constrain Σm_ν : (i) CMB (w/o lowE), (ii) CMB (w/o lowE) and DESI DR2 BAO, and (iii) CMB (w/o lowE), DESI DR2 BAO, and reionization history $x_{\text{H}_1}(z)$. We follow the method in Section 4.1 and obtain constraints on cosmological parameters (Table 4). For comparison, we also show results from CMB (w/ lowE)+BAO based on the publicly available MCMC chains provided by the DESI Collaboration. In Figure 8, we show the marginalized posterior distributions of the $(\Sigma m_\nu - \tau)$ parameters. The combination of CMB, BAO, and reionization history gives a tight upper limit on Σm_ν . The derived 95% (99%) upper limit on Σm_ν is

$$\Sigma m_\nu < 0.0550 \text{ (0.0717) eV}$$

$$(95\% \text{ (99\%)}, \text{CMB (w/o lowE) + BAO} + x_{\text{H}_1}(z)). \quad (16)$$

This upper limit is similar to the lowE result, $\Sigma m_\nu < 0.0649$ (0.0906) eV (95% (99%) limit, CMB (w/ lowE)+BAO). Although cosmological data determine upper limits on Σm_ν , lower limits are obtained from neutrino oscillation experiments. Esteban et al. (2024) report 95% lower limits of $0.058 \text{ eV} < \Sigma m_\nu$ for normal ordering (NO) and $0.098 \text{ eV} < \Sigma m_\nu$ for inverted ordering (IO), based on multiple neutrino oscillation experiments with NuFit-6.0. The cosmological upper limit is close to the lower limit for NO and well below that for IO.

First, we infer Σm_ν by combining cosmological data with neutrino oscillation constraints. In NO, the neutrino mass eigenvalues satisfy $m_1 < m_2 < m_3$. From cosmological data, the sum of these eigenvalues,

$$\Sigma m_\nu = m_1 + m_2 + m_3, \quad (17)$$

is constrained. On the other hand, neutrino oscillation experiments provide constraints on the squared mass dif-

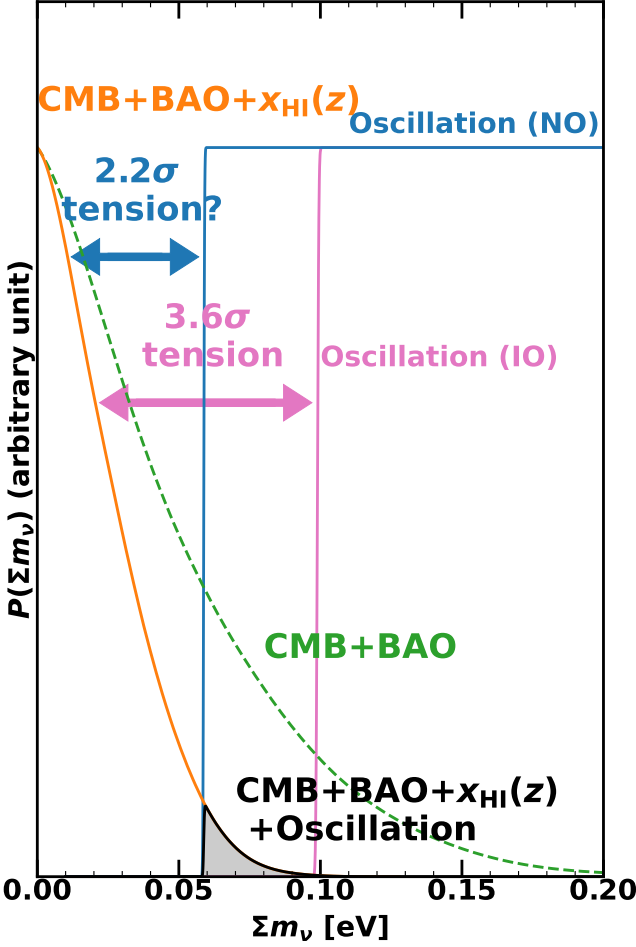


Figure 9. Marginalized posterior distributions of Σm_ν . An upper limit of $\Sigma m_\nu < 0.0550$ (0.0717) eV (95% (99%) limit) is obtained from CMB (w/o lowE)+BAO+ $x_{\text{HI}}(z)$ (orange). The blue (pink) line indicates the likelihood of Σm_ν from neutrino oscillation experiments for normal (inverted) ordering, providing a lower limit on Σm_ν . The black line shows the probability distribution of Σm_ν from the combination of cosmological data and neutrino oscillation constraints for normal ordering, which gives $\Sigma m_\nu = 0.0594^{+0.0113}_{-0.0007}$ eV. The green dashed line indicates the posterior distribution from CMB (w/o lowE)+BAO. We note that our cosmological upper limit is in 2.2σ (3.6σ) tension with the oscillation-based lower limit for normal (inverted) ordering.

ferences,

$$\Delta m_{21}^2 = m_2^2 - m_1^2 \quad \Delta m_{31}^2 = m_3^2 - m_1^2. \quad (18)$$

Here we treat Σm_ν , $\sqrt{\Delta m_{21}^2}$, and $\sqrt{\Delta m_{31}^2}$ as free parameters with the following prior distribution:

$$\begin{aligned} 0 \text{ eV} < \Sigma m_\nu < 5 \text{ eV} \\ 0 \text{ eV} < \sqrt{\Delta m_{21}^2} < 5 \text{ eV} \\ 0 \text{ eV} < \sqrt{\Delta m_{31}^2} < 5 \text{ eV} \\ \sqrt{\Delta m_{21}^2} < \sqrt{\Delta m_{31}^2} \\ \sqrt{\Delta m_{21}^2} + \sqrt{\Delta m_{31}^2} < \Sigma m_\nu \\ p(\Sigma m_\nu, \sqrt{\Delta m_{21}^2}, \sqrt{\Delta m_{31}^2}) \propto \Sigma m_\nu^{-2}. \end{aligned} \quad (19)$$

This prior ensures that m_1 remains positive, and the marginalized prior $p(\Sigma m_\nu)$ is flat, making it consistent with the priors used in our cosmological analyses. Using both cosmological and oscillation data (d_c and d_o), the posterior distribution for Σm_ν is given by

$$\begin{aligned} p(\Sigma m_\nu | d_c, d_o) &= \int d\sqrt{\Delta m_{21}^2} d\sqrt{\Delta m_{31}^2} \\ &\quad p\left(\Sigma m_\nu, \sqrt{\Delta m_{21}^2}, \sqrt{\Delta m_{31}^2} | d_c, d_o\right) \\ &\propto \int d\sqrt{\Delta m_{21}^2} d\sqrt{\Delta m_{31}^2} p(d_c | \Sigma m_\nu) \\ &\quad \times p\left(d_o | \sqrt{\Delta m_{21}^2}, \sqrt{\Delta m_{31}^2}\right) \\ &\quad \times p\left(\Sigma m_\nu, \sqrt{\Delta m_{21}^2}, \sqrt{\Delta m_{31}^2}\right), \end{aligned} \quad (20)$$

where $p(d_c | \Sigma m_\nu)$ is the cosmological likelihood, $p(d_o | \sqrt{\Delta m_{21}^2}, \sqrt{\Delta m_{31}^2})$ is obtained from the χ^2 values for neutrino mass differences (Section 2.3), and $p\left(\Sigma m_\nu, \sqrt{\Delta m_{21}^2}, \sqrt{\Delta m_{31}^2}\right)$ is the prior distribution. We evaluate the posterior distribution using the MCMC method with `emcee` (Figure 9). The mode and 68% credible interval of Σm_ν for NO are

$$\begin{aligned} \Sigma m_\nu &= 0.0594^{+0.0113}_{-0.0007} \text{ eV} \\ &\quad (\text{CMB (w/o lowE)} + \text{BAO} + x_{\text{HI}}(z) + \text{oscillation}). \end{aligned} \quad (21)$$

Although Σm_ν can be inferred for IO in a similar manner, NO is preferred over IO with a Bayes factor of 110. The above constraint corresponds to a determination of Σm_ν with 10% precision. The inferred value is close to the lower bound implied by neutrino oscillation experiments for NO, indicating that the neutrino mass spectrum is strongly hierarchical. We obtain a lower bound on the ratio of the heaviest to the lightest masses,

$m_3/m_1 > 3.7$ (95% limit), implying that m_3 accounts for most of the total mass. This result disfavors theoretical models that predict a quasi-degenerate spectrum, in which the three mass eigenvalues are nearly equal due to a small mass splitting arising from symmetry breaking (Lattanzi et al. 2020).

However, we note that our cosmological constraint favors a very small Σm_ν compared to the oscillation-based lower limit. Even for NO, our 95% upper limit of 0.0550 eV is smaller than the 95% lower limit of 0.058 eV from neutrino oscillation experiments. Our cosmological upper limit and the oscillation-based lower limit show a mild tension at the 2.2σ (3.6σ) level for NO (IO). While such a neutrino mass tension has been noted in previous studies, it was argued that it could be resolved by removing the large-scale E-mode data (Jhaveri et al. 2025). In this work, we identify the mild tension independently of large-scale E-mode measurements. This suggests that the tension may originate from systematic errors in the BAO data or from new physics. For example, neutrino decay may change the “effective” neutrino mass inferred from cosmological data. Long-range forces between dark matter particles might even make the effective neutrino mass negative by enhancing matter clustering (Craig et al. 2024). In this study, we impose a prior that restricts the neutrino mass to positive values, and investigating the results obtained with a prior that allows negative masses is left for future work. Alternatively, Λ CDM cosmology may require modification, and the dynamical dark energy model offers one possible solution (Elbers et al. 2025). This neutrino mass tension provides an independent indication of possible physics beyond Λ CDM, in either particle physics or cosmology.

7. SUMMARY AND CONCLUSION

In this paper, we present constraints on cosmological parameters using the redshift evolution of the neutral hydrogen fraction $x_{\text{H}_1}(z)$. To avoid potential biases in large-scale CMB E-mode polarization measurements due to instrumental noise or foreground subtraction, we use CMB power spectra that exclude large-scale E-mode measurements in our analyses. In addition to the CMB power spectra, we use the latest measurements of $x_{\text{H}_1}(z)$ based on Lyman- α forest data and QSO/galaxy Lyman- α damping-wing absorption measurements at $z \sim 5-14$ to determine the CMB optical depth τ . These $x_{\text{H}_1}(z)$ measurements are derived from ground-based optical and JWST observations. Since many previous results are based on the same observational data, we avoid such duplication. Our major findings are summarized below:

1. For the base- Λ CDM model, we find $\tau = 0.0552^{+0.0019}_{-0.0026}$ from CMB (w/o lowE)+ $x_{\text{H}_1}(z)$.

This result is consistent with the constraint from Planck CMB measurements including large-scale E-mode polarization. Without large-scale E-mode polarization, the addition of reionization history to CMB data improves the constraint on τ by a factor of 7.

2. There are also potential biases in $x_{\text{HI}}(z)$ measurements due to astrophysical effects. We estimate the impact of a potential absorption-model systematic as $\tau = 0.0552^{+0.0075}_{-0.0049}$ (systematics). Further investigations to quantify the impact of galaxy evolution are an important direction for future work.
3. We resolve degeneracies in the τ - Ω_m plane and find a 2.4σ tension with the DESI DR2 BAO results, which may suggest physics beyond Λ CDM, such as dynamical dark energy.
4. Allowing the sum of neutrino masses Σm_ν to vary, we derive an upper limit of $\Sigma m_\nu < 0.0550$ (0.0717) eV (95% (99%) limit) based on CMB (w/o lowE), DESI DR2 BAO, and reionization history $x_{\text{H}_1}(z)$. This result strongly supports the normal mass ordering. Furthermore, combining these results with neutrino oscillation data yields $\Sigma m_\nu = 0.0594^{+0.0113}_{-0.0007}$ eV. However, the cosmological upper limit and the oscillation-based lower limit show a 2.2σ mild tension, providing an independent indication of possible physics beyond Λ CDM.

ACKNOWLEDGMENTS

We thank Akio Inoue, Kazunori Kohri, Toshiya Namikawa, John Silverman, and Jun’ichi Yokoyama for valuable discussions on this work. This work is based on observations obtained with Planck (<http://www.esa.int/Planck>), an ESA science mission with instruments and contributions directly funded by ESA Member States, NASA, and Canada.

This research used data obtained with the Dark Energy Spectroscopic Instrument (DESI). DESI construction and operations is managed by the Lawrence Berkeley National Laboratory. This material is based upon work supported by the U.S. Department of Energy, Office of Science, Office of High-Energy Physics, under Contract No. DE-AC02-05CH11231, and by the National Energy Research Scientific Computing Center, a DOE Office of Science User Facility under the same contract. Additional support for DESI was provided by the U.S. National Science Foundation (NSF), Division of Astronomical Sciences under Contract No. AST-0950945 to the NSF’s National Optical-Infrared Astronomy Research Laboratory; the Science and Technology Facilities

Council of the United Kingdom; the Gordon and Betty Moore Foundation; the Heising-Simons Foundation; the French Alternative Energies and Atomic Energy Commission (CEA); the National Council of Humanities, Science and Technology of Mexico (CONAHCYT); the Ministry of Science and Innovation of Spain (MICINN), and by the DESI Member Institutions: www.desi.lbl.gov/collaborating-institutions. The DESI collaboration is honored to be permitted to conduct scientific research on I’oligam Du’ag (Kitt Peak), a mountain with particular significance to the Tohono O’odham Nation. Any opinions, findings, and conclusions or recommendations expressed in this material are those of the author(s) and do not necessarily reflect the views of the U.S. National Science Foundation, the U.S. Department of Energy, or any of the listed funding agencies.

This project used public archival data from the Dark Energy Survey (DES). Funding for the DES Projects has been provided by the U.S. Department of Energy, the U.S. National Science Foundation, the Ministry of Science and Education of Spain, the Science and Technology Facilities Council of the United Kingdom, the Higher Education Funding Council for England, the National Center for Supercomputing Applications at the University of Illinois at Urbana-Champaign, the Kavli Institute of Cosmological Physics at the University of Chicago, the Center for Cosmology and Astro-Particle Physics at the Ohio State University, the Mitchell Institute for Fundamental Physics and Astronomy at Texas A&M University, Financiadora de Estudos e Projetos, Fundação Carlos Chagas Filho de Amparo à Pesquisa do Estado do Rio de Janeiro, Conselho Nacional de Desenvolvimento Científico e Tecnológico and the Ministério da Ciência, Tecnologia e Inovação, the Deutsche Forschungsgemeinschaft, and the Collaborating Institutions in the Dark Energy Survey. The Collaborating Institutions are Argonne National Laboratory, the University of California at Santa Cruz, the University of Cambridge, Centro de Investigaciones Energéticas, Medioambientales y Tecnológicas-Madrid, the University of Chicago, University College London, the DES-Brazil Consortium, the University of Edinburgh, the Eidgenössische Technische Hochschule (ETH) Zürich, Fermi National Accelerator Laboratory, the University of Illinois at Urbana-Champaign, the Institut de Ciències de l’Espai (IEEC/CSIC), the Institut de Física d’Altes Energies, Lawrence Berkeley National Laboratory, the Ludwig-Maximilians Universität München and the associated Excellence Cluster Universe, the University of Michigan, the National Optical Astronomy Observatory, the University of Nottingham, The Ohio State University, the OzDES Membership Con-

sortium, the University of Pennsylvania, the University of Portsmouth, SLAC National Accelerator Laboratory, Stanford University, the University of Sussex, and Texas A&M University. Based in part on observations at Cerro Tololo Inter-American Observatory, National Optical Astronomy Observatory, which is operated by the Association of Universities for Research in Astronomy (AURA) under a cooperative agreement with the National Science Foundation.

Based on data obtained from the ESO Science Archive Facility with DOI: <https://doi.org/10.18727/archive/37>, and <https://doi.eso.org/10.18727/archive/59> and on data products produced by the KiDS consortium. The KiDS production team acknowledges support from: Deutsche Forschungsgemeinschaft, ERC, NOVA and NWO-M grants; Target; the University of Padova, and the University Federico II (Naples).

The Hyper Suprime-Cam (HSC) collaboration includes the astronomical communities of Japan and Taiwan, and Princeton University. The HSC instrumentation and software were developed by the National Astronomical Observatory of Japan (NAOJ), the Kavli Institute for the Physics and Mathematics of the Universe (Kavli IPMU), the University of Tokyo, the High Energy Accelerator Research Organization (KEK), the Academia Sinica Institute for Astronomy and Astrophysics in Taiwan (ASIAA), and Princeton University. Funding was contributed by the FIRST program from Japanese Cabinet Office, the Ministry of Education, Culture, Sports, Science and Technology (MEXT), the Japan Society for the Promotion of Science (JSPS), Japan Science and Technology Agency (JST), the Toray Science Foundation, NAOJ, Kavli IPMU, KEK, ASIAA, and Princeton University. This paper makes use of software developed for the Large Synoptic Survey Telescope. We thank the LSST Project for making their code available as free software at <http://dm.lsst.org>. The Pan-STARRS1 Surveys (PS1) have been made possible through contributions of the Institute for Astronomy, the University of Hawaii, the Pan-STARRS Project Office, the Max-Planck Society and its participating institutes, the Max Planck Institute for Astronomy, Heidelberg and the Max Planck Institute for Extraterrestrial Physics, Garching, The Johns Hopkins University, Durham University, the University of Edinburgh, Queen’s University Belfast, the Harvard-Smithsonian Center for Astrophysics, the Las Cumbres Observatory Global Telescope Network Incorporated, the National Central University of Taiwan, the Space Telescope Science Institute, the National Aeronautics and Space Administration under Grant No. NNX08AR22G issued through the Planetary Science Division of the NASA

Science Mission Directorate, the National Science Foundation under Grant No. AST-1238877, the University of Maryland, and Eotvos Lorand University (ELTE) and the Los Alamos National Laboratory. Based (in part) on data collected at the Subaru Telescope and retrieved from the HSC data archive system, which is operated by Subaru Telescope and Astronomy Data Center at National Astronomical Observatory of Japan.

This publication is based on work supported by the World Premier International Research Center Initiative (WPI Initiative), MEXT, Japan, KAKENHI (25H00674) through the Japan Society for the Promotion of Science. This work is supported by the joint research program of the Institute for Cosmic Ray Research

(ICRR), the University of Tokyo. YK and FN are supported by Forefront Physics and Mathematics Program to Drive Transformation (FoPM), a World-leading Innovative Graduate Study (WINGS) Program, the University of Tokyo. We acknowledge support from KAKENHI Grant Nos. 24KJ0668 (FN), 24KJ0575 (AM), and 25KJ0828 (MN) through Japan Society for the Promotion of Science (JSPS). FN also thank support from the ANRI Fellowship.

Software: CAMB (Lewis et al. 2000; Howlett et al. 2012), Cobaya (Torrado & Lewis 2019, 2021), emcee (Foreman-Mackey et al. 2013), GetDist (Lewis 2025), Matplotlib (Hunter 2007), NumPy (Harris et al. 2020), SciPy (Virtanen et al. 2020)

APPENDIX

A. DETAILS OF GAUSSIAN PROCESS

We use constraints on the x_{H_1} values at redshifts $\mathbf{z} = (z_1, z_2, \dots, z_n)$ to reconstruct the reionization history (Section 2.1). The probability distribution of x_{H_1} at $z = z_i$ is denoted as $p_i(x_{\text{H}_1})$, and the full set of constraints on x_{H_1} is expressed as $\{x_{\text{H}_1}\}$. Although Gaussian Process regression describes functions whose outputs can take any real value, the neutral fraction x_{H_1} is physically constrained to the range of $0 \leq x_{\text{H}_1} \leq 1$. To enforce this constraint, we introduce a latent function $f(z) \in \mathbb{R}$ and perform Gaussian process regression on $f(z)$ instead of $x_{\text{H}_1}(z)$. The conversion from $f(z)$ to $x_{\text{H}_1}(z)$ is achieved using a sigmoid function,

$$x_{\text{H}_1} = \frac{1}{1 + \exp(-f)}. \quad (\text{A1})$$

We assume a Gaussian process prior (i.e., a multivariate normal distribution) for the random variables $\mathbf{f} \equiv (f(z_1), f(z_2), \dots, f(z_n))$ at redshifts $z = z_1, z_2, \dots, z_n$:

$$f(\mathbf{z}) \sim \mathcal{N}(\mu(\mathbf{z}), k(\mathbf{z}, \mathbf{z}')). \quad (\text{A2})$$

For the mean function of the Gaussian process prior, we adopt $\mu(z) = z - 7.67$ to reflect the monotonically increasing nature of x_{H_1} . The value 7.67 corresponds to the midpoint of reionization derived from the Planck TTTEEE+lowE+lensing results (Planck Collaboration et al. 2020a). For the covariance of the Gaussian process prior, we use the radial basis function (RBF) kernel,

$$k(z, z') = s^2 \exp \left(-\frac{(\log_{10}(1+z) - \log_{10}(1+z'))^2}{2r^2} \right) + j\delta(z, z'). \quad (\text{A3})$$

Here, $j = 10^{-6}$ is included for numerical stability, and s and r are hyperparameters of the RBF kernel. We

determine these hyperparameters by maximizing the marginalized likelihood,

$$L(s, r | \{x_{\text{H}_1}\}) = \int d\mathbf{f} L(s, r, \mathbf{f} | \{x_{\text{H}_1}\}). \quad (\text{A4})$$

We obtain $s = 0.83$ and $r = 0.076$ with this procedure.

Using these hyperparameters, we perform Gaussian process regression. The posterior distribution is expressed as

$$\begin{aligned} \log(p(\mathbf{f} | \{x_{\text{H}_1}\})) &= -\frac{1}{2}(\mathbf{f} - \mu(\mathbf{z}))^T K(\mathbf{z}, \mathbf{z}')^{-1}(\mathbf{f} - \mu(\mathbf{z})) \\ &+ \sum_{i=1}^n \log \left(p_i(x_{\text{H}_1}(f(z_i))) \frac{dx_{\text{H}_1}}{df}(f(z_i)) \right) + \text{const.} \end{aligned} \quad (\text{A5})$$

We evaluate the posterior distribution of $\mathbf{f} = (f(z_1), \dots, f(z_n))$ using the MCMC method with emcee (Foreman-Mackey et al. 2013). Given the posterior distribution at $z = z_1, \dots, z_n$, we compute the values \mathbf{f}^* at new redshift points $\mathbf{z}^* = (z_1^*, \dots, z_{n'}^*)$ using the Gaussian process prior:

$$p(\mathbf{f}^* | \{x_{\text{H}_1}\}) = \int d\mathbf{f} p(\mathbf{f}^* | \mathbf{f}) p(\mathbf{f} | \{x_{\text{H}_1}\}), \quad (\text{A6})$$

where the conditional probability $p(\mathbf{f}^* | \mathbf{f})$ is given by:

$$\begin{aligned} \mathbf{f}^* | \mathbf{f} &\sim \mathcal{N}(\mu(\mathbf{z}^*) + k(\mathbf{z}^*, \mathbf{z}) k(\mathbf{z}, \mathbf{z})^{-1}(\mathbf{f} - \mu(\mathbf{z})), \\ &k(\mathbf{z}^*, \mathbf{z}^*) - k(\mathbf{z}^*, \mathbf{z}) k(\mathbf{z}, \mathbf{z})^{-1} k(\mathbf{z}, \mathbf{z}^*)). \end{aligned} \quad (\text{A7})$$

By converting \mathbf{f}^* to x_{H_1} using Equation (A1), we obtain the posterior distribution of x_{H_1} at new redshift points, $p(x_{\text{H}_1}(\mathbf{z}^*) | \{x_{\text{H}_1}\})$.

REFERENCES

Abbott, T. M. C., Aguena, M., Alarcon, A., et al. 2022a, *PhRvD*, 105, 023520, doi: [10.1103/PhysRevD.105.023520](https://doi.org/10.1103/PhysRevD.105.023520)

Abbott, T. M. C., Aguena, M., Allam, S., et al. 2022b, *PhRvD*, 105, 043512, doi: [10.1103/PhysRevD.105.043512](https://doi.org/10.1103/PhysRevD.105.043512)

Abdul Karim, M., Aguilar, J., Ahlen, S., et al. 2025a, *PhRvD*, 112, 083515, doi: [10.1103/tr6y-kpc6](https://doi.org/10.1103/tr6y-kpc6)

—. 2025b, *PhRvD*, 112, 083514, doi: [10.1103/2wwn-xjm5](https://doi.org/10.1103/2wwn-xjm5)

Allali, I. J., Singh, P., Fan, J., & Li, L. 2025, *JCAP*, 2025, 082, doi: [10.1088/1475-7516/2025/08/082](https://doi.org/10.1088/1475-7516/2025/08/082)

Amon, A., Gruen, D., Troxel, M. A., et al. 2022, *PhRvD*, 105, 023514, doi: [10.1103/PhysRevD.105.023514](https://doi.org/10.1103/PhysRevD.105.023514)

Asthana, S., Haehnelt, M. G., Kulkarni, G., et al. 2025, *MNRAS*, 542, 2968, doi: [10.1093/mnras/staf1387](https://doi.org/10.1093/mnras/staf1387)

Bennett, C. L., Larson, D., Weiland, J. L., et al. 2013, *ApJS*, 208, 20, doi: [10.1088/0067-0049/208/2/20](https://doi.org/10.1088/0067-0049/208/2/20)

Bolan, P., Lemaux, B. C., Mason, C., et al. 2022, *MNRAS*, 517, 3263, doi: [10.1093/mnras/stac1963](https://doi.org/10.1093/mnras/stac1963)

Cain, C., Scannapieco, E., McQuinn, M., D'Aloisio, A., & Trac, H. 2024, *MNRAS*, 533, L100, doi: [10.1093/mnrasl/slae067](https://doi.org/10.1093/mnrasl/slae067)

Camphuis, E., Quan, W., Balkenhol, L., et al. 2025, arXiv e-prints, arXiv:2506.20707, doi: [10.48550/arXiv.2506.20707](https://doi.org/10.48550/arXiv.2506.20707)

Carron, J., Mirmelstein, M., & Lewis, A. 2022, *JCAP*, 2022, 039, doi: [10.1088/1475-7516/2022/09/039](https://doi.org/10.1088/1475-7516/2022/09/039)

Craig, N., Green, D., Meyers, J., & Rajendran, S. 2024, *Journal of High Energy Physics*, 2024, 97, doi: [10.1007/JHEP09\(2024\)097](https://doi.org/10.1007/JHEP09(2024)097)

Curtis-Lake, E., Carniani, S., Cameron, A., et al. 2023, *Nature Astronomy*, 7, 622, doi: [10.1038/s41550-023-01918-w](https://doi.org/10.1038/s41550-023-01918-w)

Dark Energy Survey Collaboration, Abbott, T., Abdalla, F. B., et al. 2016, *MNRAS*, 460, 1270, doi: [10.1093/mnras/stw641](https://doi.org/10.1093/mnras/stw641)

Davies, F. B., Bosman, S. E. I., D'Odorico, V., et al. 2026, *MNRAS*, 545, staf1862, doi: [10.1093/mnras/staf1862](https://doi.org/10.1093/mnras/staf1862)

Delouis, J.-M., Pagano, L., Mottet, S., Puget, J.-L., & Vibert, L. 2019, *A&A*, 629, A38, doi: [10.1051/0004-6361/201834882](https://doi.org/10.1051/0004-6361/201834882)

Du, G.-H., Li, T.-N., Wu, P.-J., Zhang, J.-F., & Zhang, X. 2025, arXiv e-prints, arXiv:2507.16589, doi: [10.48550/arXiv.2507.16589](https://doi.org/10.48550/arXiv.2507.16589)

Efstathiou, G., & Gratton, S. 2021, *The Open Journal of Astrophysics*, 4, 8, doi: [10.21105/astro.1910.00483](https://doi.org/10.21105/astro.1910.00483)

Elbers, W. 2025, arXiv e-prints, arXiv:2508.21069, doi: [10.48550/arXiv.2508.21069](https://doi.org/10.48550/arXiv.2508.21069)

Elbers, W., Aviles, A., Noriega, H. E., et al. 2025, *PhRvD*, 112, 083513, doi: [10.1103/w9pk-xsk7](https://doi.org/10.1103/w9pk-xsk7)

Esteban, I., Gonzalez-Garcia, M. C., Maltoni, M., et al. 2024, *Journal of High Energy Physics*, 2024, 216, doi: [10.1007/JHEP12\(2024\)216](https://doi.org/10.1007/JHEP12(2024)216)

Fausey, H. M., Vejlgaard, S., van der Horst, A. J., et al. 2025, *MNRAS*, 536, 2839, doi: [10.1093/mnras/stae2757](https://doi.org/10.1093/mnras/stae2757)

Finkelstein, S. L., D'Aloisio, A., Paardekooper, J.-P., et al. 2019, *ApJ*, 879, 36, doi: [10.3847/1538-4357/ab1ea8](https://doi.org/10.3847/1538-4357/ab1ea8)

Flaugher, B., Diehl, H. T., Honscheid, K., et al. 2015, *AJ*, 150, 150, doi: [10.1088/0004-6256/150/5/150](https://doi.org/10.1088/0004-6256/150/5/150)

Foreman-Mackey, D., Hogg, D. W., Lang, D., & Goodman, J. 2013, *PASP*, 125, 306, doi: [10.1086/670067](https://doi.org/10.1086/670067)

Garcia-Gallego, O., Iršič, V., Haehnelt, M. G., & Bolton, J. S. 2025, arXiv e-prints, arXiv:2510.00107, doi: [10.48550/arXiv.2510.00107](https://doi.org/10.48550/arXiv.2510.00107)

Greig, B., Mesinger, A., Davies, F. B., et al. 2022, *MNRAS*, 512, 5390, doi: [10.1093/mnras/stac825](https://doi.org/10.1093/mnras/stac825)

Greig, B., Mesinger, A., Bañados, E., et al. 2024, *MNRAS*, 530, 3208, doi: [10.1093/mnras/stae1080](https://doi.org/10.1093/mnras/stae1080)

Gunn, J. E., & Peterson, B. A. 1965, *ApJ*, 142, 1633, doi: [10.1086/148444](https://doi.org/10.1086/148444)

Harris, C. R., Millman, K. J., van der Walt, S. J., et al. 2020, *Nature*, 585, 357, doi: [10.1038/s41586-020-2649-2](https://doi.org/10.1038/s41586-020-2649-2)

Howlett, C., Lewis, A., Hall, A., & Challinor, A. 2012, *JCAP*, 2012, 027, doi: [10.1088/1475-7516/2012/04/027](https://doi.org/10.1088/1475-7516/2012/04/027)

Hunter, J. D. 2007, *Computing in Science and Engineering*, 9, 90, doi: [10.1109/MCSE.2007.55](https://doi.org/10.1109/MCSE.2007.55)

Ishigaki, M., Kawamata, R., Ouchi, M., et al. 2018, *ApJ*, 854, 73, doi: [10.3847/1538-4357/aaa544](https://doi.org/10.3847/1538-4357/aaa544)

Jhaveri, T., Karwal, T., & Hu, W. 2025, *PhRvD*, 112, 043541, doi: [10.1103/6vd2-rbfm](https://doi.org/10.1103/6vd2-rbfm)

Jin, X., Yang, J., Fan, X., et al. 2023, *ApJ*, 942, 59, doi: [10.3847/1538-4357/aca678](https://doi.org/10.3847/1538-4357/aca678)

Jones, G. C., Bunker, A. J., Saxena, A., et al. 2025, *MNRAS*, 536, 2355, doi: [10.1093/mnras/stae2670](https://doi.org/10.1093/mnras/stae2670)

Jung, I., Finkelstein, S. L., Dickinson, M., et al. 2020, *ApJ*, 904, 144, doi: [10.3847/1538-4357/abbd44](https://doi.org/10.3847/1538-4357/abbd44)

Kageura, Y., Ouchi, M., Nakane, M., et al. 2025, *ApJS*, 278, 33, doi: [10.3847/1538-4365/adc690](https://doi.org/10.3847/1538-4365/adc690)

Kallosh, R., & Linde, A. 2025, *General Relativity and Gravitation*, 57, 135, doi: [10.1007/s10714-025-03470-6](https://doi.org/10.1007/s10714-025-03470-6)

Lattanzi, M., Gerbino, M., Freese, K., Kane, G., & Valle, J. W. F. 2020, *Journal of High Energy Physics*, 2020, 213, doi: [10.1007/JHEP10\(2020\)213](https://doi.org/10.1007/JHEP10(2020)213)

Lewis, A. 2025, *JCAP*, 2025, 025, doi: [10.1088/1475-7516/2025/08/025](https://doi.org/10.1088/1475-7516/2025/08/025)

Lewis, A., Challinor, A., & Lasenby, A. 2000, *ApJ*, 538, 473, doi: [10.1086/309179](https://doi.org/10.1086/309179)

Liu, R., Zhu, Y., Hu, W., & Miranda, V. 2025, arXiv e-prints, arXiv:2510.14957, doi: [10.48550/arXiv.2510.14957](https://doi.org/10.48550/arXiv.2510.14957)

Lodha, K., Calderon, R., Matthewson, W. L., et al. 2025, *PhRvD*, 112, 083511, doi: [10.1103/w4c6-1r5j](https://doi.org/10.1103/w4c6-1r5j)

Louis, T., La Posta, A., Atkins, Z., et al. 2025, *JCAP*, 2025, 062, doi: [10.1088/1475-7516/2025/11/062](https://doi.org/10.1088/1475-7516/2025/11/062)

Madhavacheril, M. S., Qu, F. J., Sherwin, B. D., et al. 2024, *ApJ*, 962, 113, doi: [10.3847/1538-4357/acff5f](https://doi.org/10.3847/1538-4357/acff5f)

Mason, C. A., Chen, Z., Stark, D. P., et al. 2025, arXiv e-prints, arXiv:2501.11702, doi: [10.48550/arXiv.2501.11702](https://doi.org/10.48550/arXiv.2501.11702)

Mason, C. A., Naidu, R. P., Tacchella, S., & Leja, J. 2019a, *MNRAS*, 489, 2669, doi: [10.1093/mnras/stz2291](https://doi.org/10.1093/mnras/stz2291)

Mason, C. A., Treu, T., Dijkstra, M., et al. 2018, *ApJ*, 856, 2, doi: [10.3847/1538-4357/aab0a7](https://doi.org/10.3847/1538-4357/aab0a7)

Mason, C. A., Fontana, A., Treu, T., et al. 2019b, *MNRAS*, 485, 3947, doi: [10.1093/mnras/stz632](https://doi.org/10.1093/mnras/stz632)

Matthee, J., Naidu, R. P., Pezzulli, G., et al. 2022, *MNRAS*, 512, 5960, doi: [10.1093/mnras/stac801](https://doi.org/10.1093/mnras/stac801)

McDonough, E., & Ferreira, E. G. M. 2025, arXiv e-prints, arXiv:2512.05108, doi: [10.48550/arXiv.2512.05108](https://doi.org/10.48550/arXiv.2512.05108)

McGreer, I. D., Mesinger, A., & D’Odorico, V. 2015, *MNRAS*, 447, 499, doi: [10.1093/mnras/stu2449](https://doi.org/10.1093/mnras/stu2449)

Miyatake, H., Sugiyama, S., Takada, M., et al. 2023, *PhRvD*, 108, 123517, doi: [10.1103/PhysRevD.108.123517](https://doi.org/10.1103/PhysRevD.108.123517)

More, S., Sugiyama, S., Miyatake, H., et al. 2023, *PhRvD*, 108, 123520, doi: [10.1103/PhysRevD.108.123520](https://doi.org/10.1103/PhysRevD.108.123520)

Muñoz, J. B., Mirocha, J., Chisholm, J., Furlanetto, S. R., & Mason, C. 2024, *MNRAS*, 535, L37, doi: [10.1093/mnrasl/slae086](https://doi.org/10.1093/mnrasl/slae086)

Naidu, R. P., Tacchella, S., Mason, C. A., et al. 2020, *ApJ*, 892, 109, doi: [10.3847/1538-4357/ab7cc9](https://doi.org/10.3847/1538-4357/ab7cc9)

Nakane, M., Ouchi, M., Nakajima, K., et al. 2024, *ApJ*, 967, 28, doi: [10.3847/1538-4357/ad38c2](https://doi.org/10.3847/1538-4357/ad38c2)

Namikawa, T. 2025, *PhRvL*, 135, 161004, doi: [10.1103/qgnn-6hsf](https://doi.org/10.1103/qgnn-6hsf)

Naokawa, F., Namikawa, T., Murai, K., Obata, I., & Kamada, K. 2024, arXiv e-prints, arXiv:2405.15538, doi: [10.48550/arXiv.2405.15538](https://doi.org/10.48550/arXiv.2405.15538)

Napolitano, L., Pentericci, L., Dickinson, M., et al. 2025, arXiv e-prints, arXiv:2508.14171, doi: [10.48550/arXiv.2508.14171](https://doi.org/10.48550/arXiv.2508.14171)

Ouchi, M., Harikane, Y., Shibuya, T., et al. 2018, *PASJ*, 70, S13, doi: [10.1093/pasj/psx074](https://doi.org/10.1093/pasj/psx074)

Pagano, L., Delouis, J.-M., Mottet, S., Puget, J.-L., & Vibert, L. 2020, *A&A*, 635, A99, doi: [10.1051/0004-6361/201936630](https://doi.org/10.1051/0004-6361/201936630)

Paoletti, D., Hazra, D. K., Finelli, F., & Smoot, G. F. 2025, *PhRvD*, 111, 043532, doi: [10.1103/PhysRevD.111.043532](https://doi.org/10.1103/PhysRevD.111.043532)

Planck Collaboration, Ade, P. A. R., Aghanim, N., et al. 2014, *A&A*, 571, A16, doi: [10.1051/0004-6361/201321591](https://doi.org/10.1051/0004-6361/201321591)

Planck Collaboration, Adam, R., Aghanim, N., et al. 2016a, *A&A*, 596, A108, doi: [10.1051/0004-6361/201628897](https://doi.org/10.1051/0004-6361/201628897)

Planck Collaboration, Ade, P. A. R., Aghanim, N., et al. 2016b, *A&A*, 594, A13, doi: [10.1051/0004-6361/201525830](https://doi.org/10.1051/0004-6361/201525830)

Planck Collaboration, Aghanim, N., Ashdown, M., et al. 2016c, *A&A*, 596, A107, doi: [10.1051/0004-6361/201628890](https://doi.org/10.1051/0004-6361/201628890)

Planck Collaboration, Aghanim, N., Akrami, Y., et al. 2020a, *A&A*, 641, A6, doi: [10.1051/0004-6361/201833910](https://doi.org/10.1051/0004-6361/201833910)

—. 2020b, *A&A*, 641, A1, doi: [10.1051/0004-6361/201833880](https://doi.org/10.1051/0004-6361/201833880)

—. 2020c, *A&A*, 641, A5, doi: [10.1051/0004-6361/201936386](https://doi.org/10.1051/0004-6361/201936386)

Qin, Y., Mesinger, A., Prelogović, D., et al. 2025, *PASA*, 42, e049, doi: [10.1017/pasa.2025.35](https://doi.org/10.1017/pasa.2025.35)

Qu, F. J., Sherwin, B. D., Madhavacheril, M. S., et al. 2024, *ApJ*, 962, 112, doi: [10.3847/1538-4357/acfe06](https://doi.org/10.3847/1538-4357/acfe06)

Rinaldi, P., Caputi, K. I., Costantin, L., et al. 2023, *ApJ*, 952, 143, doi: [10.3847/1538-4357/acdc27](https://doi.org/10.3847/1538-4357/acdc27)

Rosenberg, E., Gratton, S., & Efstathiou, G. 2022, *MNRAS*, 517, 4620, doi: [10.1093/mnras/stac2744](https://doi.org/10.1093/mnras/stac2744)

Sailer, N., Farren, G. S., Ferraro, S., & White, M. 2025, arXiv e-prints, arXiv:2504.16932, doi: [10.48550/arXiv.2504.16932](https://doi.org/10.48550/arXiv.2504.16932)

Secco, L. F., Samuroff, S., Krause, E., et al. 2022, *PhRvD*, 105, 023515, doi: [10.1103/PhysRevD.105.023515](https://doi.org/10.1103/PhysRevD.105.023515)

Shimizu, S., Kashikawa, N., Kikuta, S., et al. 2025, *MNRAS*, 542, 3125, doi: [10.1093/mnras/staf1377](https://doi.org/10.1093/mnras/staf1377)

Sims, P. H., Bevins, H. T. J., Fialkov, A., et al. 2025, *MNRAS*, 544, 3856, doi: [10.1093/mnras/staf1864](https://doi.org/10.1093/mnras/staf1864)

Sobacchi, E., & Mesinger, A. 2015, *MNRAS*, 453, 1843, doi: [10.1093/mnras/stv1751](https://doi.org/10.1093/mnras/stv1751)

Spergel, D. N., Verde, L., Peiris, H. V., et al. 2003, *ApJS*, 148, 175, doi: [10.1086/377226](https://doi.org/10.1086/377226)

Sugiyama, S., Miyatake, H., More, S., et al. 2023, *PhRvD*, 108, 123521, doi: [10.1103/PhysRevD.108.123521](https://doi.org/10.1103/PhysRevD.108.123521)

Tada, Y., & Terada, T. 2024, *PhRvD*, 109, L121305, doi: [10.1103/PhysRevD.109.L121305](https://doi.org/10.1103/PhysRevD.109.L121305)

Tan, J. C., & Komatsu, E. 2025, arXiv e-prints, arXiv:2510.19647, doi: [10.48550/arXiv.2510.19647](https://doi.org/10.48550/arXiv.2510.19647)

Tang, M., Stark, D. P., Topping, M. W., Mason, C., & Ellis, R. S. 2024, *ApJ*, 975, 208, doi: [10.3847/1538-4357/ad7eb7](https://doi.org/10.3847/1538-4357/ad7eb7)

The Dark Energy Survey Collaboration. 2005, arXiv e-prints, astro, doi: [10.48550/arXiv.astro-ph/0510346](https://doi.org/10.48550/arXiv.astro-ph/0510346)

Torrado, J., & Lewis, A. 2019, Cobaya: Bayesian analysis in cosmology, *Astrophysics Source Code Library*, record ascl:1910.019. <http://ascl.net/1910.019>

—. 2021, *JCAP*, 2021, 057, doi: [10.1088/1475-7516/2021/05/057](https://doi.org/10.1088/1475-7516/2021/05/057)

Totani, T., Kawai, N., Kosugi, G., et al. 2006, *PASJ*, 58, 485, doi: [10.1093/pasj/58.3.485](https://doi.org/10.1093/pasj/58.3.485)

Totani, T., Aoki, K., Hattori, T., et al. 2014, *PASJ*, 66, 63, doi: [10.1093/pasj/psu032](https://doi.org/10.1093/pasj/psu032)

Tristram, M., Banday, A. J., Górski, K. M., et al. 2021, *A&A*, 647, A128, doi: [10.1051/0004-6361/202039585](https://doi.org/10.1051/0004-6361/202039585)

—. 2022, *PhRvD*, 105, 083524, doi: [10.1103/PhysRevD.105.083524](https://doi.org/10.1103/PhysRevD.105.083524)

Tristram, M., Banday, A. J., Douspis, M., et al. 2024, *A&A*, 682, A37, doi: [10.1051/0004-6361/202348015](https://doi.org/10.1051/0004-6361/202348015)

Umeda, H., Ouchi, M., Kageura, Y., et al. 2025a, arXiv e-prints, arXiv:2504.04683, doi: [10.48550/arXiv.2504.04683](https://doi.org/10.48550/arXiv.2504.04683)

Umeda, H., Ouchi, M., Kikuta, S., et al. 2025b, *ApJS*, 277, 37, doi: [10.3847/1538-4365/adb1c0](https://doi.org/10.3847/1538-4365/adb1c0)

Ďurovčíková, D., Eilers, A.-C., Chen, H., et al. 2024, *ApJ*, 969, 162, doi: [10.3847/1538-4357/ad4888](https://doi.org/10.3847/1538-4357/ad4888)

Virtanen, P., Gommers, R., Oliphant, T. E., et al. 2020, *Nature Medicine*, 17, 261, doi: [10.1038/s41592-019-0686-2](https://doi.org/10.1038/s41592-019-0686-2)

Wang, F., Davies, F. B., Yang, J., et al. 2020, *ApJ*, 896, 23, doi: [10.3847/1538-4357/ab8c45](https://doi.org/10.3847/1538-4357/ab8c45)

Whitler, L. R., Mason, C. A., Ren, K., et al. 2020, *MNRAS*, 495, 3602, doi: [10.1093/mnras/staa1178](https://doi.org/10.1093/mnras/staa1178)

Wold, I. G. B., Malhotra, S., Rhoads, J., et al. 2022, *ApJ*, 927, 36, doi: [10.3847/1538-4357/ac4997](https://doi.org/10.3847/1538-4357/ac4997)

Wright, A. H., Kuijken, K., Hildebrandt, H., et al. 2024, *A&A*, 686, A170, doi: [10.1051/0004-6361/202346730](https://doi.org/10.1051/0004-6361/202346730)

Wright, A. H., Stölzner, B., Asgari, M., et al. 2025, *A&A*, 703, A158, doi: [10.1051/0004-6361/202554908](https://doi.org/10.1051/0004-6361/202554908)

Zhu, Y., Becker, G. D., Bosman, S. E. I., et al. 2022, *ApJ*, 932, 76, doi: [10.3847/1538-4357/ac6e60](https://doi.org/10.3847/1538-4357/ac6e60)